EXAMINING THE SUBSTRATE SPECIFICITY OF THE ENZYME 3-O-SULFOTRANSFERASE THAT REGULATES THE BIOSYNTHESIS OF THE ANTICOAGULANT HEPARAN SULFATE

by

JOO KYUNG KIM

(Under the Direction of Robert J. Woods)

ABSTRACT

Heparan sulfate (HS) is a highly sulfated glycosaminoglycan (GAG) that affects a wide range of physiopathological functions. Its diverse functionality stems from the varying sulfation patterns along the polysaccharide chain. The current techniques for identifying the sequence of HS on the cell surface are limited. Thus, the goal of this project was to exploit the substrate specificity of the enzyme 3-O-sulfotransferase isoform 1 (3-OST 1) for the development of the HS binding probe that would recognize the anticoagulant HS. Thereby, molecular dynamics (MD) simulations and MM-GBSA analysis were performed to examine the structure and the free energy between 3-OST 1 and the 3-O-sulfated HS. In order to convert the 3-OST 1 into high-affinity binding probe, site-directed mutagenesis was performed on the catalytic glutamic acid (E90) residue and the effects of the mutations in binding to HS fragments were investigated by Bio-Layer Interferometry (BLI) analysis.

INDEX WORDS: Carbohydrate, Heparan Sulfate, Heparan Sulfate Proteoglycan, Sulfotransferase, Site-Directed Mutagenesis, Molecular Dynamics, MM-GBSA, Bio-Layer interferometry

EXAMINING THE SUBSTRATE SPECIFICITY OF THE ENZYME 3-O-SULFOTRANSFERASE THAT REGULATES THE BIOSYNTHESIS OF THE ANTICOAGULANT HEPARAN SULFATE

by

JOO KYUNG KIM

B.S., Mars Hill University, 2013

A Thesis Submitted to the Graduate Faculty of The University of Georgia in Partial Fulfillment of the Requirements for the Degree

MASTER OF SCIENCE

ATHENS, GEORGIA

2017

EXAMINING THE SUBSTRATE SPECIFICITY OF THE ENZYME 3-O-SULFOTRANSFERASE THAT REGULATES THE BIOSYNTHESIS OF THE ANTICOAGULANT HEPARAN SULFATE

by

JOO KYUNG KIM

Major Professor:	Robert J. Woods
Committee:	Robert S. Haltiwanger
	Kelley Moremen
	Lianchun Wang

Electronic Version Approved:

Suzanne Barbour
Dean of the Graduate School
The University of Georgia
December 2017

ACKNOWLEDGEMENTS

I want to thank my major professor Dr. Robert J Woods who gave me the opportunity to investigate the heparan sulfate glycosaminoglycan and guided me through the graduate study. I also would like to express my gratitude to the current and previous Woods' group members, who made this journey more delightful. I am thankful for Dr. Kelley Moremen, Dr. Lianchun Wang, and Dr. Robert S. Haltiwanger who served as my committee members. I would like to thank my family who have supported and trusted me through it all. Friends, I am so grateful for each one and all of you. Without your contribution, I would not have made to this point. Last but not least, thank you NCA family. You take a special place in my heart.

TABLE OF CONTENTS

Page

LIST OF TABLES

Page

LIST OF FIGURES

Page

CHAPTER 1

SUMMARY

Heparan sulfate (HS) is a linear polysaccharide that is ubiquitously present on the cell surface or the ECM of the mammalian cell. HS consists of repeating disaccharide units of glucuronic acids (GlcA) or iduronic acid (IdoA) and glucosamine [1,2]. HS displays structural heterogeneity and depending on the sulfation patterns, HS contributes to various physiological and pathological processes, such as cellular differentiation, migration of tumor cells, and regulating adhesion [1,2,5]. Current techniques for identifying the sequences of HS on the surfaces of the cells are limited; monoclonal anti-HS antibodies have been employed to detect specific HS epitopes in the tissues. Anti-HS antibodies identify the general changes in sulfation, however, but most fail to differentiate between specific sulfation patterns along the polysaccharide chain [28]. Therefore, the overall aim of this project was to develop a reagent that would recognize and bind to a specific sulfation patterns of HS from a catalytically inactive sulfotransferase. Thus, the substrate specificity of the enzyme 3-O-sulfotransferase isoform 1 (3-OST 1) that is involved in the last step of the HS biosynthetic pathway was exploited for the development of HS binding probes.

From the ternary crystal structure of the 3-OST 1 with 3′-phosphoadenosine 5′-phosphate (PAP) and heptasaccharide substrate (PDB ID: 3UAN) complex, a glutamic acid (E90) has been proposed to act as the catalytic residue that is essential for the sulfotransferase activity (shown in Figure 1) [26]. In order to convert the 3-OST 1 into high-affinity binding probe that would bind

the anticoagulant 3-O-sulfated HS with enhanced affinity, the structure and the free energy of the 3-OST 1 and the 3-O-sulfated HS fragment complex was investigated by Molecular Dynamics (MD) simulations and mm-GBSA analysis. Then site-directed mutagenesis was used to replace the catalytic glutamic acid residue by the polar glutamine, basic histidine, basic arginine, and basic lysine residues to enhance the affinity of the 3-OST 1 towards the 3-O-sulfated HS fragment. The hypothesis was that replacing the carboxyl group of E90 with the polar and basic residues, the negative charge-to-charge interaction between the carboxyl group of E90 and the 3-O-sulfated position of the anticoagulant HS would be alleviated. Thereby, the catalytically inactive 3-OST 1 mutants could be converted into a high-affinity binding probe that targets the anticoagulant HS.

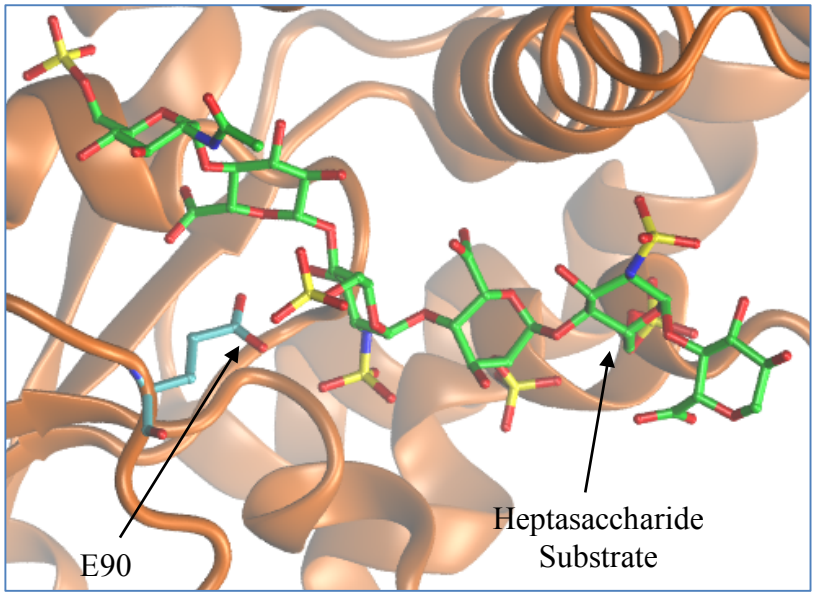

Figure 1. 3-OST 1 BINDING SITE. The crystal structure of the 3-OST 1(shown in new cartoon representation-orange) in complex with the heptasaccharide ligand substrate (shown in stick representation-green). In the substrate binding site, the catalytic residue E90 (indicated in cyan) was identified within hydrogen bonding distance (2.7 A) from the acceptor 3-OH group [26]. For this project, the catalytic residue was submitted to SDM analysis to exploit the substrate specificity of 3-OST 1.

CHAPTER 2

LITERATURE REVIEW

2.1 HEPARN SULFATE AND HEPARIN

Heparan sulfate (HS) is a glycosaminoglycan (GAG) that consists of repeating disaccharide units of glucosamine and uronic acids (Figure 2). HS is widely present on the mammalian cell surfaces or the extracellular matrix. HS interacts with various proteins, such as enzymes, enzyme inhibitors, growth factors, cytokines, chemokines, and extracellular matrix proteins [4,7]. Thereby, HS participates in various physiopathological functions, such as cell proliferation, immunity, blood coagulation, and metastasis of the cells [1,2,8,12].

HS biosynthesis initiates in the Golgi apparatus when the HS oligosaccharide core chain that consists of Xyl-Gal-Gal-GlcA is attached to a protein core. As shown in Figure 3, the HS chain is elongated by repeating disaccharide units of 1-4- linked glucosamine and glucuronic acids using the nucleotide sugars imported from the cytoplasm. Then the polymerized HS chains are modified by a number of sulfotransferases and an epimerase; the N-acetyl-D-glucosamine residues are selectively deacetylated and the amino groups are selectively sulfated [6]. Some of the D-glucuronic acids are epimerized to L-iduronic acids at C5 positions. A number of sulfotransferase add sulfo group to the hydroxyl groups in the C3 and C6 positions of the glucosamine residues. Also, some of the hydroxyl groups in the C2 position of iduronic acids are sulfated [1,4,26].

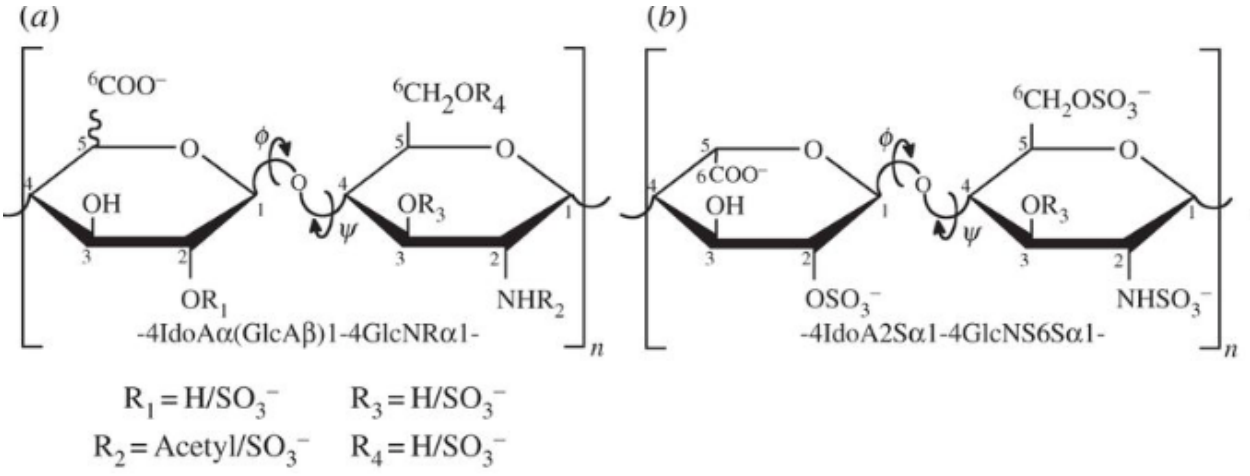

Figure 2. THE MAIN BUILDING BLOCKS OF HEPARAN SULFATE.

Heparan sulfate consists of repeating disaccharide units of 1-4- linked glucosamine and uronic acids. Each one of the monosaccharides of HS can be sulfated and the uronic acids can be epimerized. The modifications occur in no template manner. Thus, the HS chains display difference in the degree of modification depending on the cell type that HS is expressed. Variation is also observed in the glycosidic linkage torsion angles. The iduronic acids have been observed both in the skew-boat ($^2S_0$) and chair ($^1C_4$) conformations. Therefore, the iduronic acids enhance the HS conformational flexibility. (a) The most common disaccharide unit observed in HS. (b) the most common disaccharide unit of heparin that is produced in the mast cells. From: Meneghetti MC, Hughes AJ, Rudd TR, Nader HB, Powell AK, Yates EA, Lima MA. Heparan sulfate and heparin interactions with proteins. Journal of The Royal Society Interface. 2015 Sep 6;12(110):20150589

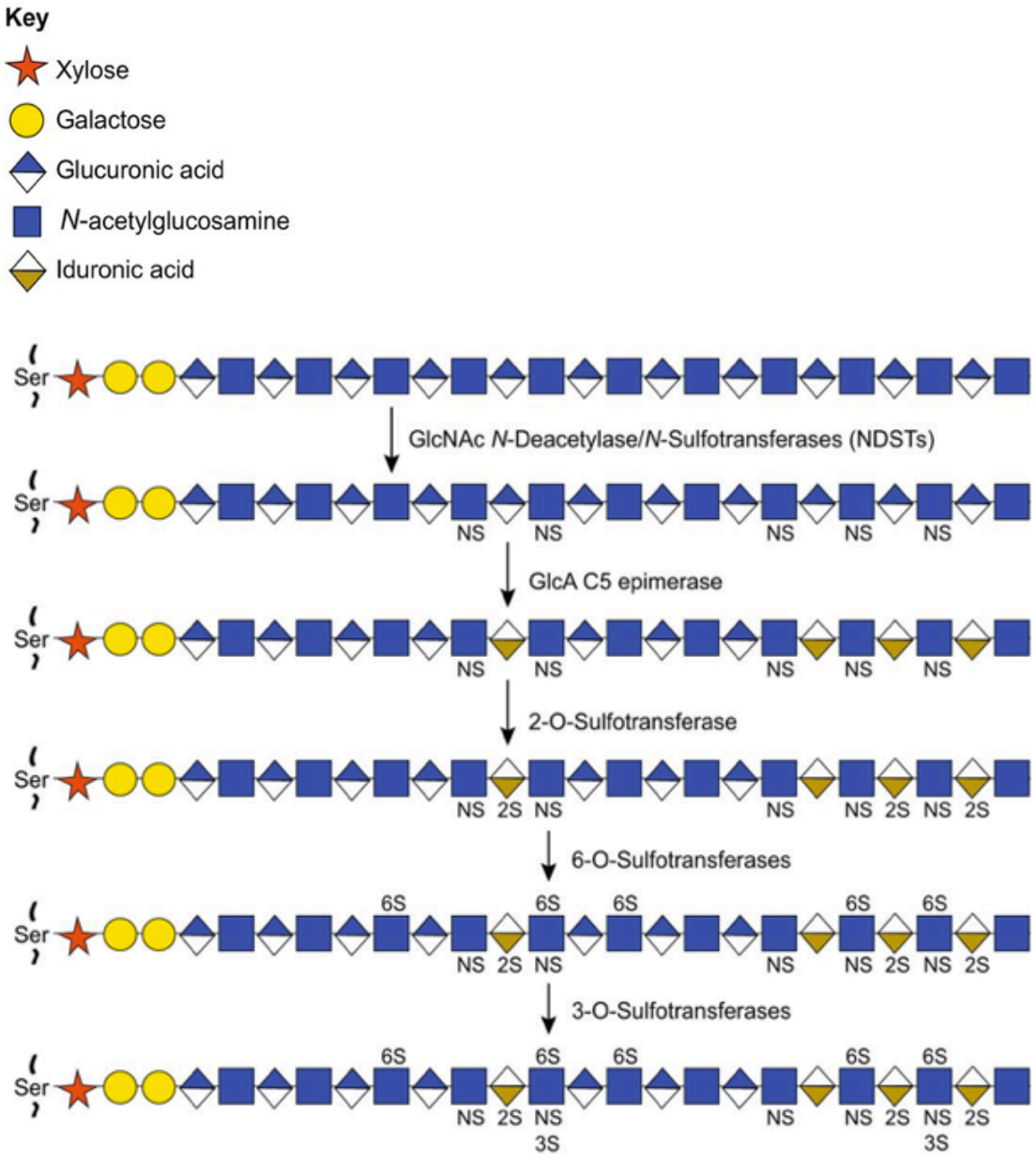

Figure 3. HS BIOSYNTHETIC PATHWAY.

HS biosynthesis occur in the order that is indicated. Once the HS chains are elongated, some of the acetyl groups are removed and replaced by the sulfate group in N -acetylglucosamine residues. Then a number of glucuronic acids are epimerized to iduronic acids. After the epimerization, a number of sulfotransferase replace the OH groups with sulfate group. From: Poulain FE, Yost HJ. Heparan sulfate proteoglycans: a sugar code for vertebrate development. Development. 2015 Oct 15;142(20):3456-67.

HS is synthesized in all of the animal cells in the order that is indicated in the Figure 3. However, the modifications occur in no template manner and fail to go to completion [6,7]. The resultant heterogeneous HS chain can be divided into various domains depending on the degree of modification (Figure 4); HS chains consist of domains that contain clusters of N- sulfated (NS domain) residues, N- acetylated (NA domain) residues, and mixed domains (NA/NS domains) [2]. The variation in the HS chain length, degree of the modified residues, and spacing of the of the sulfated domains are observed in different cell types at different times in development [6]. The availability of the precursors, the specificity of the biosynthetic enzymes, and flux through the Golgi apparatus dictate the size and composition of HS in different cells [14].

Heparin is the highly sulfated and iduronic acid-rich form of HS. As shown in Figure 5, heparin contains the same monosaccharide building block as HS. However, heparin displays higher degree of N- and O- sulfation; on average HS contain $\geq$1 sulfate group per disaccharide, whereas heparin contains an average of 2.7 negative charges [8,9]. In addition, heparin displays higher degree of epimerization of glucuronic acids.

HS is synthesized on the mast cells [8,9];multiple heparin chains are attached to the protein core on the cell surface, but an HS-degrading endoglucuronidase cleave the heparin proteoglycans and produce the heparin chains that are much smaller (12 to 14kDa) than the HS (20-100kDa) in size [13, 42]. Heparin polysaccharides are then stored in the cytoplasmic secretory granules [44]. Since 1935, heparin obtained from the porcine intestine or bovine lung has been extensively used as an anticoagulant drug [26, 44]. The anticoagulant HS contains a unique pentasaccharide sequence that may bind and activate the antithrombin (AT) to display the anticoagulant activity (shown in Figure 5) [12]. The naturally obtained heparin is processed by

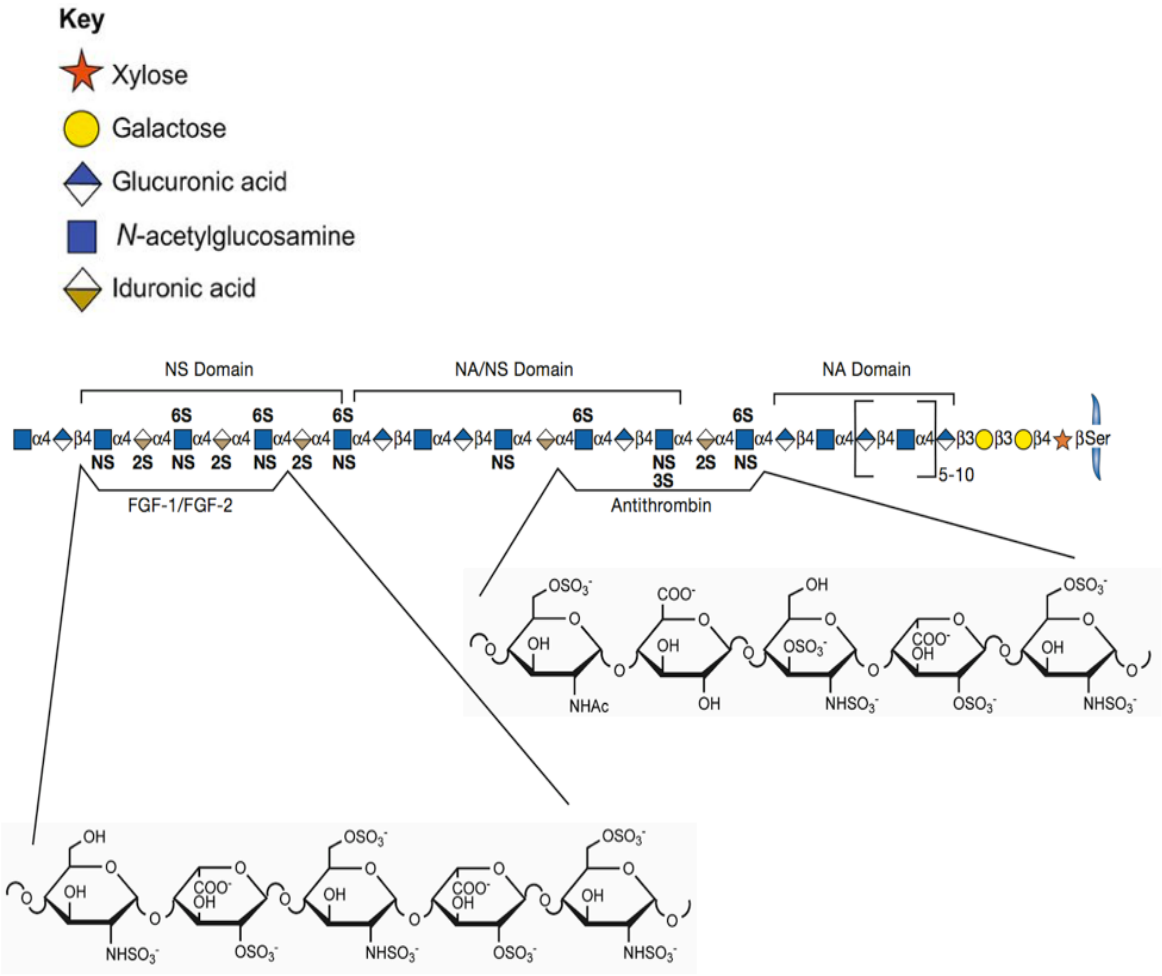

Figure 4. HEPARAN SULFATE DOMAINS.

Depending on the degree of sulfation and epimerization various domains are present in the HS chain. The N-sulfate domain (NS), N-acetyalted domain (NA), and the mixed domains act as binding sites for various ligands. Antithrombin and fibroblast growth factors recognize and form a complex with specific sequences along the HS chain. From: Esko JD, Kimata K, Lindahl U. Proteoglycans and Sulfated Glycosaminoglycans. In: Varki A, Cummings RD, Esko JD, et al., editors. Essentials of Glycobiology. 2nd edition. Cold Spring Harbor (NY): Cold Spring Harbor Laboratory Press; 2009. Chapter 16.

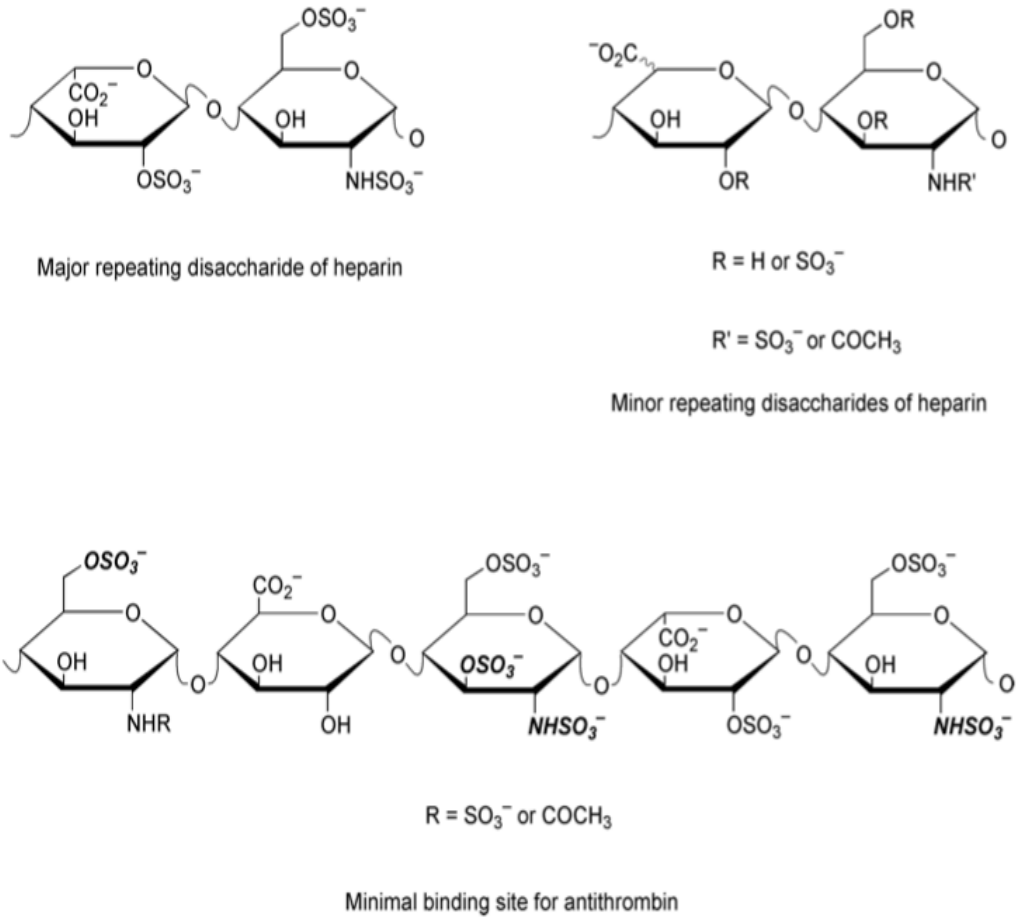

Figure 5. BUILDING BLOCKS OF HEPARIN.

In heparin, the glucosamine residues display higher degree of sulfation; the rare 3-O-sulfation of the glucosamine residues are more common than the HS that are produced by different cell types. Also, heparin displays higher degree of epimerization. The pentasaccharide shown on the bottom is the unique pentasaccharide within heparin that acts as the binding site for antithrombin. When the unique pentasaccharide sequence is present within heparin, the affinity to AT and the anticoagulant activity is increased. The pentasaccharide are synthesized and sold as an anticoagulant drug called Arixtra. From: Rabenstein DL. Heparin and heparan sulfate: structure and function. Natural product reports. 2002;19(3):312-31.

an extensive purification process before it is used in medical practice [12], however, the distribution of contaminated heparin in 2007 had a worldwide detrimental impact. As an alternative, the unique pentasaccharide anticoagulant HS sequence that binds to antithrombin has been synthesized and sold as an anticoagulant drug called Arixta. The synthetic analog Arixtra has been administered for the prophylaxis and/or treatment of DVT or pulmonary embolism [15].

2.2 HEPARAN SULFATE PROTEOGLYCANS (HSPG)

On the membrane or the extracellular matrix of animal cells, one or multiple linear HS chains that are covalently attached to the serine residue of the protein core and form the heparan sulfate proteoglycans (HSPG) [5]. HSPG can be divided to three subfamilies depending on the structure of the protein core that is associated with the cell membrane; syndecans and betaglycans contain a transmembrane domain, glypicans are connected to the membrane through a glycophosphatidylinositol (GPI) anchor, whereas other HSPG such as agrin and perlecans are secreted into the extracellular matrix [2,14].

HSPG are among the most negatively charged biopolymers and participates in various physical and the pathological functions, since the structural diversity enables the HS fragments to interact with various proteins, such as enzymes, enzyme inhibitors, growth factors, cytokines, chemokines, and extracellular matrix proteins [4,7]. HS contributes to various functions by dictating the localization of heparan sulfate binding proteins (HSBP) at specific sites, protection of HSBP from proteolysis, formation of the complexes for signaling pathways, protein oligomerization, and allosteric activation of the protein [13].

Biochemical and biophysical studies have shown that specificity and affinity between HS and HSBP are demonstrated at many different levels [2,3,14]. Some proteins such as

antithrombin require specific HS modifications, whereas other proteins such as IL8 interact with specific domain structure of HS. Other proteins such as thrombin, display nonspecific interactions with the HS that are based on the charge interactions [3,13]. The highly anionic charged sulfate groups and the orientation of the carboxyl groups dictate the specificity of ligand interactions [43]; due to the anionic nature of HS polysaccharides, electrostatic interactions are important in the binding of HS to HSBP [10, 13]. In addition to the electrostatic interactions, van der Waals (VDW) forces and hydrophobic interactions with the carbohydrate backbone have been reported to contribute to the binding interactions by 10–40% [3, 14].

The current techniques to examine the HSPG in situ are limited. Monoclonal anti-HS antibodies have been developed to assess the occurrence and localization of HS in tissues, however, most fail to differentiate between specific sulfation patterns [28]. Thus, the goal of this study was to develop the HS binding probe that would target specific sulfation pattern in the HS from the catalytically inactive HS sulfotransferases. The enzymes from the biosynthetic pathway of HS already recognize a specific substrate, thus the inherent specificity of the enzyme was exploited for the development of high-affinity binding probe that would target a unique sulfation pattern of HS; either the substrate or the product of the enzymatic reaction. In this project, the catalytically inactive 3-OST 1was selected to develop the high-affinity probe that would recognize the product of the 3-OST 1 activity; the anticoagulant HS.

2.3 3-O-SULFOTRANSFERASE ISOFORM 1 (3-OST 1)

3-O-sulfotransferase isoform 1 (3-OST 1) belongs to the 3-OST family that is involved in the last step of the HS biosynthetic pathway. Seven isoforms of the 3-OST families (3-OST 1, 2,

3a, 3b, 4, 5, and 6) are known to transfer a sulfo group (SO3) to the C3 position of a glucosamine unit [26, 32-34]. Each one of the isoforms display subtle differences in the substrate preferences; as presented in Figure 6, 3-OST 1 transfers the sulfo group to the glucosamine unit that is linked to a GlcA unit, whereas 3-OST 3, 3-OST 2, 3-OST 4, and 3-OST 6 isoforms sulfates the glucosamine residue that is linked to an IdoUA2S unit. 3-OST 5 sulfates the 3-OH of the glucosamine that is linked to GlcA, IdoA, or IdoA2S [26].

The HS products modified by various isoforms perform distinct biological functions [25] such as anticoagulant activity [25], the entry of herpes simplex virus into host cells to establish infection [33], growth of neurons, and it controls the progenitor cell expansion [26]. The biosynthesis of specific 3-O-sulfated HS is regulated by the expression level of the specific 3-OST isoforms and the defined substrate specificities that each one of the 3-OST isoforms display. The exact mechanisms that dictate the substrate specificity of 3-OST isoforms are still being investigated [47].

In this project, the substrate specificity of the 3-OST 1 enzyme that regulates the biosynthesis of the anticoagulant HS was exploited. 3-OST 1 was selected for the development of the high-affinity probe since it interacts with sulfation patterns of biological significance. The product of the 3-OST 1 enzymatic activity is the anticoagulant HS that is recognized by antithrombin. Thereby, the mechanism of 3-OST 1 enzymatic activity has been characterized. As shown in Figure 7, 3-OST 1 transfers the sulfate group from the donor substrate 3'-phosphoadenosine-5'- phosphosulfate (PAPS) to the 3- OH position of the glucosamine residue generating 3'-phosphoadenosine-5'-phosphate (PAP) as a by-product. The crystal structure of the enzyme 3-OST 1 that was obtained in ternary complex with 3′-phosphoadenosine 5′-

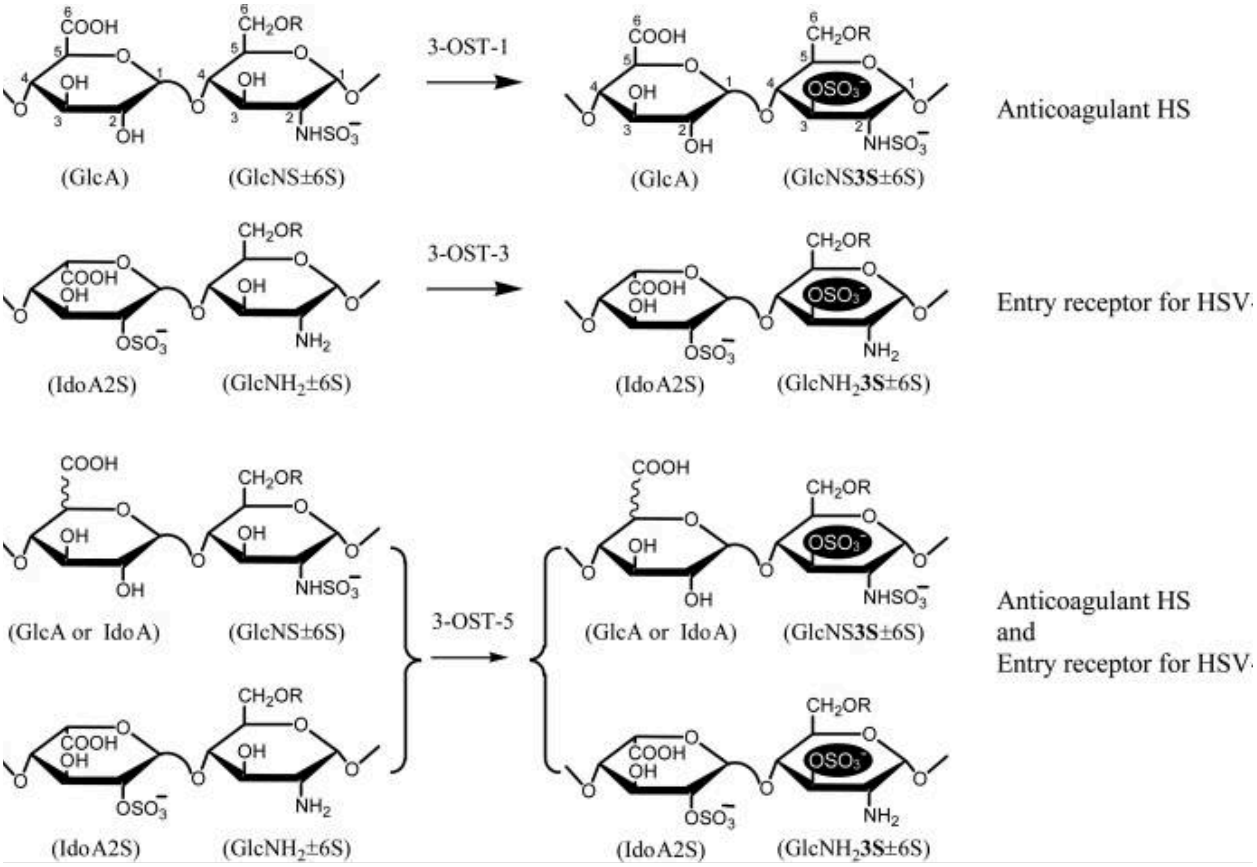

Figure 6. SUBSTATE SPECIFICITY OF THE 3-OST ISOFORMS.

Each one of the isoforms recognize and sulfate different substrates. 3-OST isoform 1 sulfates the 3-OH position of the glucosamine residue that is linked to GlcA residue, whereas 3-OST isoform 3 sulfates the glucosamine residue that is linked to an IdoA2S. 3-OST isoform 5 sulfates the 3-OH of the glucosamine that is linked to GlcA, IdoA, or IdoA2S. The HS fragments modified by different isoforms perform distinct biological functions. The sulfate group that is added to C3 positions from the 3-OST1are indicated in black. From: Ding XU, Tiwari V, Guoqing XI, Clement C, Shukla D, Jian LI. Characterization of heparan sulfate 3-O-sulphotransferase isoform 6 and its role in assisting the entry of herpes simplex virus type 1. Biochemical Journal. 2005 Jan 15;385(2):451-9.

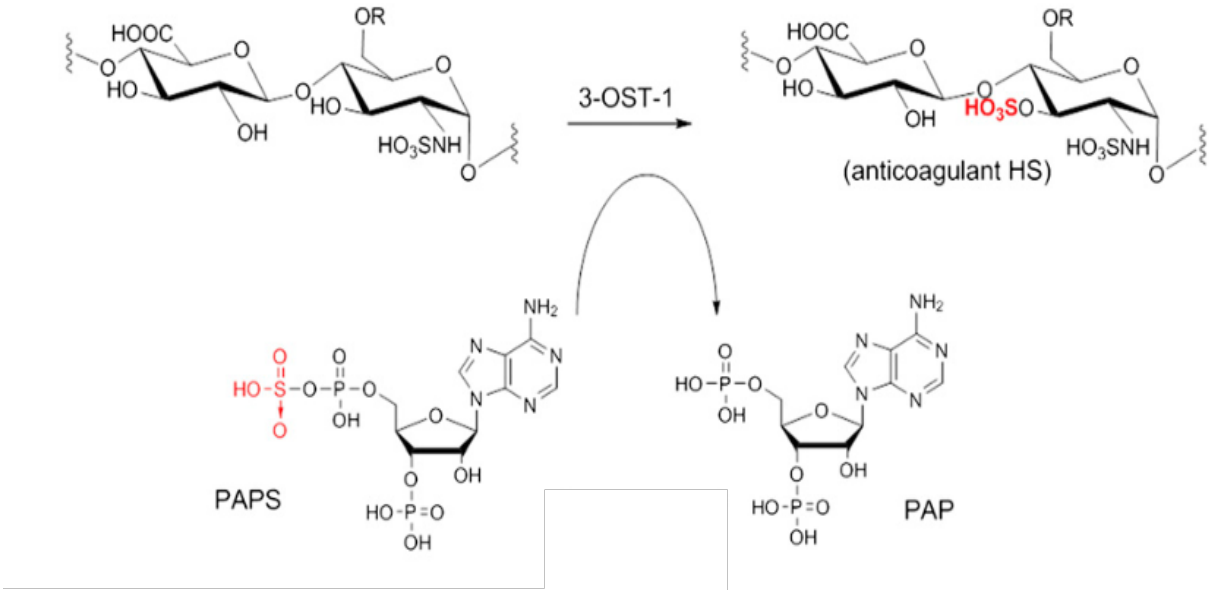

Figure 7. REACTION CATALYZED BY 3-OST 1.

3-OST 1 sulfates the glucosamine that is flanked by a GlcA on its non-reducing end. 3-OST 1 transfers the sulfate group (indicated in red) from the donor substrate 3'-phosphoadenosine-5'-phosphosulfate (PAPS) to the 3- OH position of the glucosamine residue generating 3'-phosphoadenosine-5'-phosphate (PAP) as a by-product. From: Moon AF, Xu Y, Woody SM, Krahn JM, Linhardt RJ, Liu J, Pedersen LC. Dissecting the substrate recognition of 3-O-sulfotransferase for the biosynthesis of anticoagulant heparin. Proceedings of the National Academy of Sciences. 2012 Apr 3;109(14):5265-70.

phosphate (PAP) and heptasaccharide substrate has provided atomic level information on the structure of the conserved sulfotransferase domain that consist of α/β motif and a phosphosulfate binding loop [26]. The crystal structures and the mutagenesis analysis have shown that the conserved glutamic acid (E90) that is found inside of the large cleft acts as the catalytic residue for the 3-OST 1 activity.

The catalytic mechanism of the 3-OST 1 is similar to estrogen sulfotransferase (EST) [32]. Similar to EST, the catalytic activity occurs through SN-2 like displacement mechanism. A conserved glutamate (E90) has been proposed to serve as the catalytic base for the 3-OST 1 activity and deprotonates the nucleophilic acceptor 3-OH group of the glucosamine residue. Then the deprotonated hydroxyl group attacks the sulfur atom of the PAPS in order to form a transition state between the donor PAPS and the acceptor group. A conserved lysine residue (K68) of the phosphate-binding loop stabilizes the negative charge that is built on the leaving PAP group. As a result, the lysine residue forms a hydrogen bond between the oxygen of the acceptor group and the sulfur atom of the sulfate group [32].

2.4 GOAL OF THE PROJECT

The goal of this study was to develop the high-affinity probe from the catalytically inactive HS sulfotransferases. The enzymes from the biosynthetic pathway of HS already recognize a specific substrate, thus the inherent specificity of the enzyme was exploited for the development of high-affinity binding probe that would target a unique sulfation pattern of HS; either the substrate or the product of the enzymatic reaction. In this project, the catalytically inactive 3-OST 1was selected to develop the high-affinity probe that would recognize the anticoagulant HS, the enzymatic product of the 3-OST 1 reaction.

High-affinity binding probes that differentiate between sulfation patterns of HS could be applied into the currently existing antibody mediated assays and applications. The reagent can be used to create an affinity column by conjugating the probe to a resin. The columns could be used for the chromatographic purification of the anticoagulant HS/heparin. Also, the reagents could be labeled by fluorescent tags for in situ histological applications that would identify and track the changes in specific sulfation patterns over time for disease diagnosis and therapy.

In this thesis, the development of high-affinity binding reagent that would target the anticoagulant HS is presented. In chapter 3, Molecular Dynamics (MD) simulations and MM-GBSA analysis was performed to examine the structure and the free energy of the 3-OST 1 and the anticoagulant HS complex. Then in chapter 4, the 3-OST 1 enzymes were submitted to mutagenesis, expression, and purification processes. The negatively charged carboxyl group of the E90 residue was substituted by positively charged (arginine, lysine, and histidine) and polar (glutamine) residues; E90K/ E90H/ E90R/E90Q in order to enhance the affinity of the reagents to the anticoagulant HS. The central hypothesis was that the binding affinity could be enhanced by replacing the catalytic residue to the positively charged residues. The affinity and the specificity of the mutants towards HS fragments were assessed by BLI analysis.

.

CHAPTER 3

MD SIMULATION AND MM-GBSA ANALYSIS

In this chapter, the 3-OST 1 and the HS ligand complex was investigated by Molecular Dynamics (MD) simulations. The coordinates of the protein were obtained from the crystal structure of 3-OST 1 (Protein Data Bank ID: 3UAN [26]), whereas the natural HS substrate was replaced by Arixtra, the synthetic analogue of the 3-O-sulfated product of the 3-OST 1 enzymatic activity. AMBER softwatre package [56] and the GLYCAM 06 force field [49] were used to examine the binding interaction of the complex. The free energy (ΔG_{bind}) of the 3-OST 1 and ligand complex was calculated from the MM-GBSA analysis to determine the per-residue molecular mechanical (MM) contribution. The contribution of each residue to the total ΔG_{bind} was calculated to identify the residues that contribute the most favorably and unfavorably to the binding interactions.

3.1 MD SIMULATION

For the molecular modeling, the interactions in the system can be computed by the quantum mechanics (QM) and the molecular mechanic force field (MM). The quantum mechanical description (QM) are used to calculate the rearrangement of the electrons during a chemical reaction [48], whereas the molecular mechanic (MM) force field uses the Newtonian and the classical physics to calculate positions and the velocities of each atoms in the system [46]. MD simulations are the standard methods for simulating the motions of biomolecules using the

laws of classical physics [48]. The potential energies of the atoms are calculated by the force fields (equation 1.a) that include the intramolecular interactions (bond and angles) modeled by harmonic functions and the torsions that are modeled by periodic functions [48]. The intermolecular Van der Waals interactions (short-range repulsion and the long-range attraction) are modelled by the Lennard- Jones potential. The electrostatic interaction between the charged atoms are calculated by the Coulomb's law (equation 1.b) [48].

$$PE = V_{tot} = \sum_{bonds} V_r + \sum_{angles} V_\theta + \sum_{torsions} V_\tau + \sum_{atoms} V_{vanderWaals} + \sum_{atoms} V_{electrostatics} \quad (1.a)$$

$$V_{total} = \sum_{bonds} K_r(r - r_{eq})^2 + \sum_{angles} K_\theta(\theta - \theta_{eq})^2 + \sum_{dihedrals} \sum_{n} \frac{V_n}{2}\left[1 + \cos(n\phi - \gamma_n)\right] + \sum_{\substack{non-bonded \\ i<j}} \left[\frac{A_{ij}}{R_{ij}^{12}} - \frac{C_{ij}}{R_{ij}^{6}} + \frac{q_i q_j}{\varepsilon R_{ij}}\right] \quad (1.b)$$

In this project, the changes in the conformation of the 3-OST1 and HS fragment complex was examined over time. In order to calculate the new position of the particles after the time (Δt), the Taylor expansion equation was used (equation 2) [53], where the position(x) of the particles were assigned from the experimental structural data that are available on Protein Data Bank (www.rcsb.org).

$$x(t + \Delta t) = x(t) + v(t)\,\Delta t + \frac{1}{2}a(t)\,\Delta t^2 + \ldots \quad (2)$$

During the MD simulation, the potential energy of the system was recalculated at each time step for all of the atoms in the systems in their new position by the force field [46]. Then, using the Newton's second law (Equation 3) the atomic accelerations were computed, using the forces derived from the change in the potential energies "∂V" and their new positions were calculated at each time step (Equation 2).

$$F_i = - \frac{\partial V}{\partial xi} = m_i a_i \quad (3)$$

3.2 MM-GBSA ANALYSIS

In order to quantify the free energy of the carbohydrate-protein interactions, post-processing analysis Molecular Mechanics Generalized Born Surface Area (MM-GBSA) were employed. MMGBSA analysis exploits the molecular mechanics and implicit solvation models to calculate the binding free energies [41]. The relative and absolute binding free energies were calculated by replacing the explicit water molecules with an implicit model. The continuum solvent model was used since they reduce the time that is required for the calculation of the binding free energies and the errors that are derived by statistical averaging of the solvent conformations [41].

$\Delta G_{binding}$ between HS and the 3OST1 was calculated using the equation (4), where the contribution from solvation was calculated by the generalized Born implicit solvation models [51]. The average molecular mechanical energy (E_{MM}) that incorporates the contributions from the angle, torsions, van der Waals interaction between the solvent and solute, and electrostatic was calculated from the trajectories obtained from the snapshots of the ligand-receptor interactions [41]. Therefore, by calculating the contribution of each residue to the binding energy, the residues that are important for the binding interaction in a protein-carbohydrate complex were identified [46].

$$\Delta G_{binding} = \Delta G_{complex} - \Delta G_{cootein} - \Delta G_{ligand} \quad (4)$$

$$\Delta G_{binding} = \Delta H - T\Delta S \simeq \Delta E_{MM} + \Delta G_{desol} - T\Delta S \quad (5)$$

$$\Delta E_{MM} \simeq \Delta E_{internal} + \Delta E_{electrostatic} + \Delta E_{VDW} \quad (6)$$

3.3 MATERIAL AND METHODS

A crystal structure of the 3-OST 1 protein (Protein Data Bank ID: 3UAN) reported at 1.84 Å resolution was used as a starting structure in this analysis [26]. All the crystallized ligands (3′-phosphoadenosine 5′-phosphate and heptasaccharide substrate) and water molecules were removed. The natural HS substrate was replaced with Arixtra, the pentasaccharide, synthetic analog that represents the 3-O-suflated product of 3-OST 1 enzymatic reaction. The topology and coordinate files of the ligand was prepared using the tLeap program of the AMBER software suite. For the simulations, the protein structure was solvated in a truncated octahedral box of TIP3P water molecules with counter ions (Na^+) added to neutralize the charge, using the tLeap module of AMBER.

The simulations were performed using AMBER12 force field [56] with ff14SB[57] and GLYCAM 06 parameters [49] for the amino acids and carbohydrate residues with a cutoff for nonbonded interactions of 10 Å. The system was minimized in two step protocols to remove the mad contacts. Initially, the energy of the water and ions was minimized while keeping all protein atoms restrained. This step was followed by energy minimization of the entire system. Each minimization comprised an initial phase of steepest descent method for 1000 steps, followed by conjugate gradient for 24000 steps. The resulting minimized structures were subjected to MD simulation performed with the pmemd.cuda version of AMBER12 [56]. Electrostatic interactions were calculated by the Particle-Mesh Ewald (PME) procedure that calculated the infinite range Coulomb interaction under periodic boundary conditions (PBC) [50]. A cutoff for nonbonded interactions was set to 8 Å. The SHAKE algorithm was employed to constrain hydrogen-containing bonds, enabling an integration time step of 2 fs. The system was heated to 300 K under NVT conditions over 60 ps by employing the Berendsen thermostat with a coupling time

constant of 1 ps and allowed to equilibrate for a total of 1 ns under NPT conditions. A post-equilibration data set was collected for 100 ns, under NPT conditions.

The interaction energy of the complex was computed with the single-trajectory Molecular Mechanics-Generalized Born Solvent Accessible Surface Area method [58] using the MPBSA.py.MPI module [56]. Before the analyses, all water molecules and ions were removed from each complex, and the contribution from desolvation approximated through the GB implicit solvation model (igb = 2) [59]. The simulation was divided into 5-ns bins, and average interaction energy contributions were computed from an ensemble of 100 snapshots evenly distributed within each bin.

3.4 RESULTS AND DISCUSSION

The initial atomic coordinates of the wild-type 3-o-sulfotransferase was obtained from the ternary crystal structure of the protein with 3´-phosphoadenosine 5´-phosphate (PAP) and heptasaccharide substrate at a resolution of 1.84 $\AA$ (PDB ID: 3UAN) [26]. For the simulations, the heptasaccharide substrate from the original crystal structure was replaced by the 3-O-sulfated Arixtra in order to examine the contribution of the C3 sulfate group in the binding interaction of the complex. The pentasaccharide analog of the 3-OST 1 product (Arixtra) was used, since the hydrogen bonding interactions were observed only between five saccharides and the binding cleft in the 3-OST1 crystal structure [26].

The trajectory files that contained all the coordinates of each atom were collected for 100ns. In order to examine, if the binding interaction between the 3-OST 1 and ligand Arixta had converged, the RMSD values of the ligand with respect to the starting structure was calculated. RMSD monitors the change in the atomic position x_i in reference to the starting position x_o

(equation 7). Based on the changes in the RMSD values over the 100ns simulation, the system had not converged. As shown in Figure 7a, towards the end of the simulation the RMSD value of the ligand with respect to the starting structure increased, thus the simulation was performed for an additional 100ns time period. Performing the simulation for a longer time period is common, depending on the nature and the object of the study. During the additional production step, the RMSD values decreased and converged (shown in Figure 7b).

$$RMSD = \sqrt{\frac{\sum_{i=1}^{N}(x_i - x_o)^2}{N}} \quad (7)$$

Once the system reached statistical equilibration, the trajectory data of each atom in the system were collected and characterized by Molecular Mechanics-Generalized Born Surface Area (MM-GBSA). MM-GBSA analysis quantified the energy of carbohydrate-protein interactions at per-residue level to examine how each of the residues contribute to the binding interactions [46]. The amino acid residues were ranked based on the total $\Delta G_{bind.}$ and the residues that are favorable or unfavorable for the binding interactions were identified.

In table 1, the residues that contribute the most favorably for the binding interactions between 3-OST1 and Arixtra are presented. Based on the MM-GBSA analysis, the amino acids that are involved in the substrate binding at the catalytic site contribute the most favorably to the binding interactions (shown in Figure 9). The polar and positively charged amino acid residues (presented in table 1) have previously been reported to interact with the carboxyl and the sulfate group of the substrate in the binding site to enhance the binding affinity of the enzyme-ligand complex [26,32,47].

The residues that are the most unfavorable for the binding interaction of the 3-OST 1 with Arixtra are presented in table 2. The negatively charged glutamic and aspartic acid residues

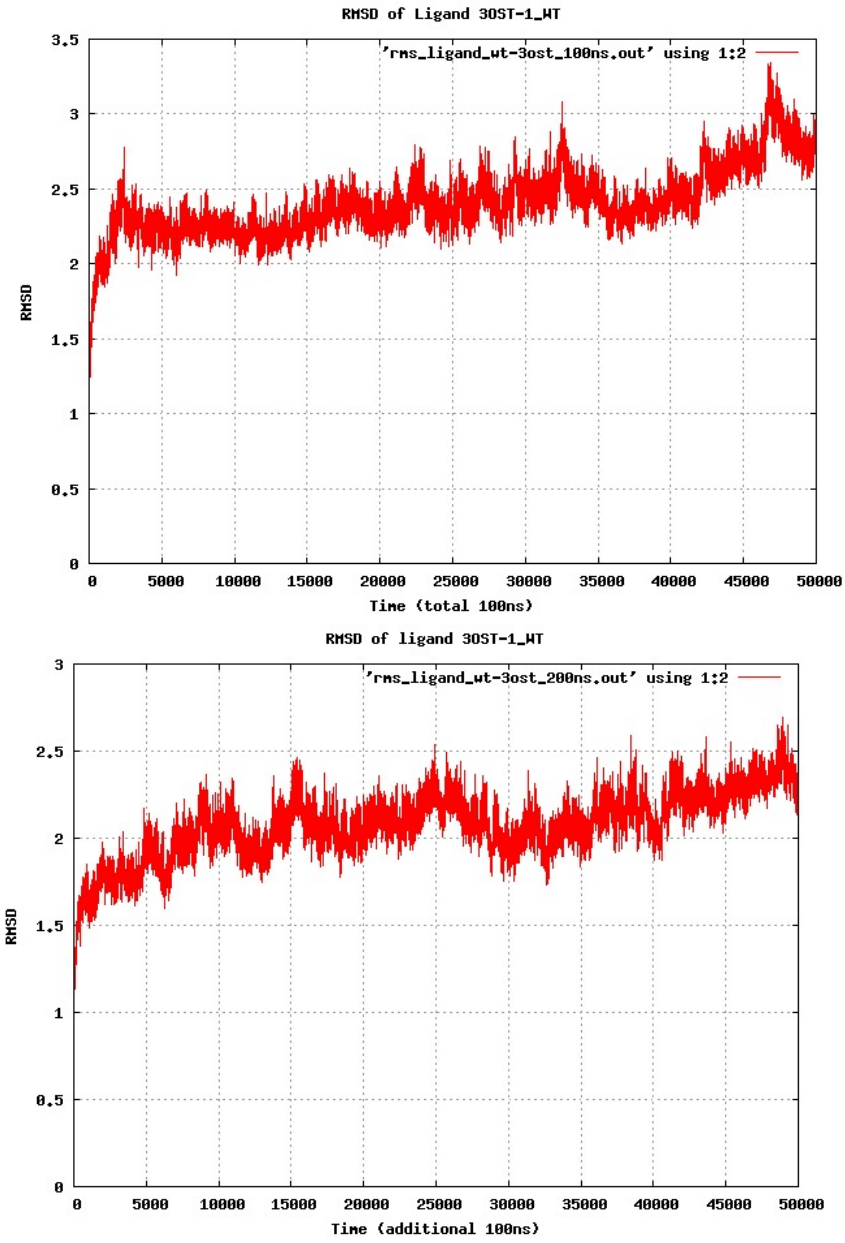

FIGURE 8. THE RMSD VALUE OF THE LIGAND.

Over the time course of the simulation, trajectory files that contain the coordinates of atoms were collected. In order to examine if the complex had converged, the RMSD values of the ligand atoms were plotted over time in reference to the starting position $x_{o.}$ During the initial 100ns simulation the RMSD value had not converged (Figure 7a, shown on the top). Thus, the complex was simulated for an additional 100ns. Once the system reached statistical equilibration (Figure 7b, shown on the bottom), the trajectory data of each atom in the system were collected and characterize by MM-GBSA analysis.

Residue	van der Waals	Electrostatic	Polar Desolvation	Nonpolar Desolvation	Total ΔG_{bind}
ARG 67	-3.21	-217.60	205.11	-0.37	-16.07
ARG 72	-1.89	-180.19	173.44	-0.52	-9.15
LYS 68	-1.25	-216.71	209.71	-0.33	-8.58
ASN 167	-1.37	-16.23	10.74	-0.33	-7.19
GLN 163	-2.31	-13.10	9.55	-0.26	-6.12
ARG 276	-1.36	-173.31	170.43	-0.29	-4.54
ARG 268	-0.09	-117.37	113.37	-0.09	-4.18
LYS 173	-0.08	-98.14	97.06	-0.01	-1.17

Table 1. MOST FAVORABLE RESIDUES FOR THE BINDING INTERACTIONS.

From the MM-GBSA analysis the contributions of each atom to the ligand-receptor interaction were calculated per-residue energy contributions (kcal/mol). The residues of the 3-OST 1 that contribute the most favorably based on the energy cut-off of -1kcal/mol are presented. The positively charged lysine, arginine, and polar histidine residues contribute positively to the binding interactions.

Residue	van der Waals	Electrostatic	Polar Desolvation	Nonpolar Desolvation	Total ΔG_{bind}
GLU 90	-0.48	152.15	3.73	-144.68	3.15
ASP 95	-0.11	123.64	2.13	-119.38	2.00
ASP 160	-0.23	152.74	2.19	-148.36	1.97
GLU 88	-0.14	123.19	1.93	-119.33	1.79
GLU 272	-0.20	110.03	1.93	-106.16	1.73
GLU 76	-0.56	118.67	2.15	-114.37	1.56
GLU 122	-0.04	107.80	1.47	-104.86	1.44
GLU 155	-0.01	90.38	1.18	-88.03	1.16
GLU 97	-0.02	84.30	1.15	-82.00	1.13

Table 2. MOST UNFAVORABLE RESIDUES FOR THE BINDING INTERACTIONS.

Residues that are the most repulsive to the binding interactions were identified from the MM-GBSA analysis. The residues of the 3-OST 1 that contribute the most unfavorably based on the energy cut-off of 1kcal/mol are presented. It is notable that the negatively charged glutamic acid and aspartic acid residues contribute the most negatively to the binding interactions.

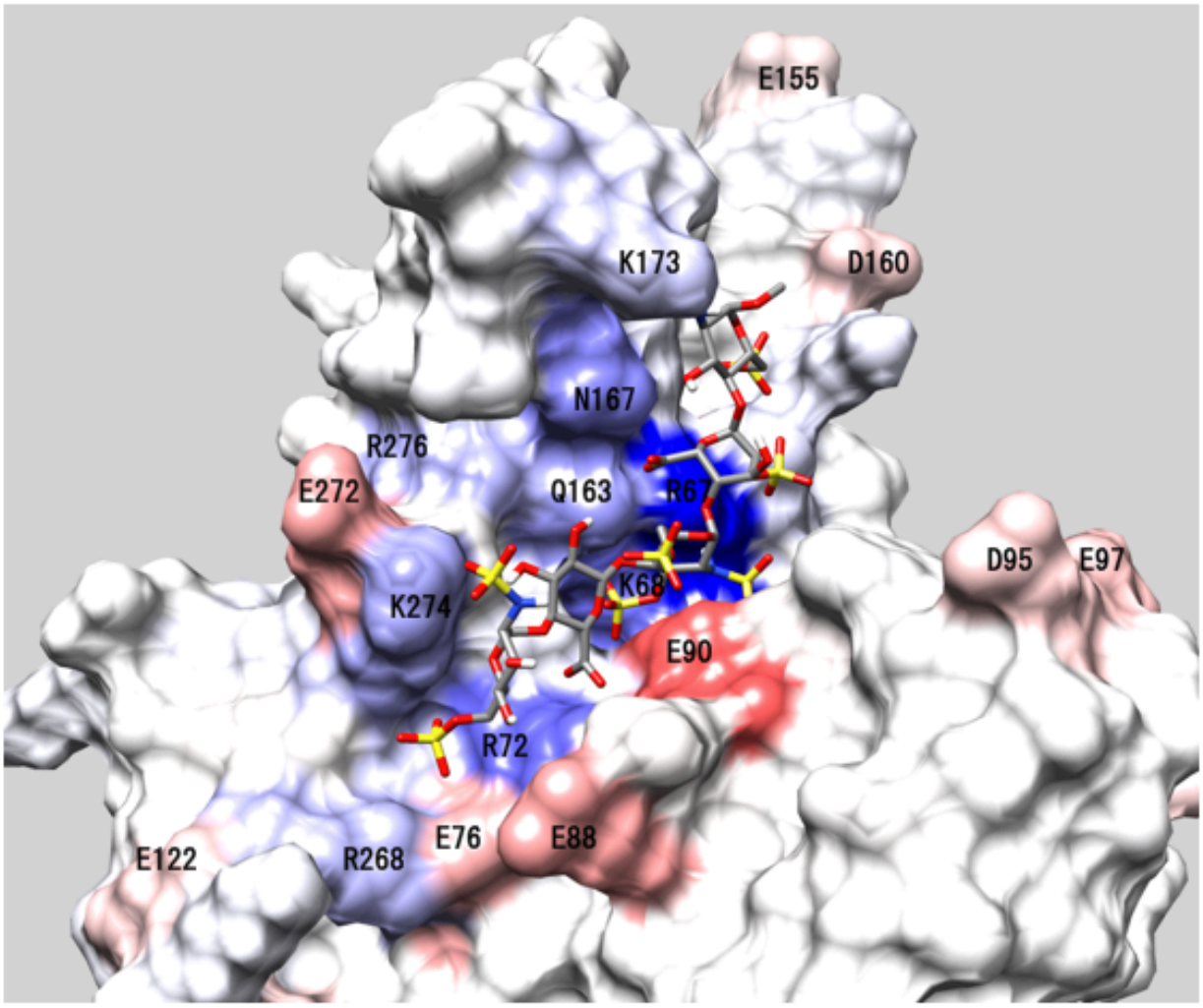

FIGURE 9. THE CONTRIBUTION OF THE 3-OST 1 RESIDUES TO THE LIGAND BINDING. The amino acids were color-coded based on the per-residue binding free energies(ΔG_{bind}) that were calculated from the MM-GBSA analysis of the 3-OST 1 and Arixta complex. Based on the ΔG_{bind} values the most attractive residues (indicated in blue) are the polar and positively charged residues that are clustered in the 3-OST 1 binding site. The most unfavorable residues for the binding interactions are the glutamic and aspartic residues shown in red. As listed in table 2, the catalytic residue (E90) was identified as the most repulsive residue in binding to Arixtra. Therefore, E90 was selected for mutagenesis to enhance the affinity of the 3-OST 1 towards the 3-O-sulfated HS.

are the most unfavorable to the binding interaction. The carboxyl group of the negatively charged amino acid residues and the negatively charged sulfate groups of the ligands were speculated to repulse each other. In particular, the catalytic residue E90 was identified to be the most repulsive residue for binding to Arixtra, due to the charge repulsion between the glutamic acid and the 3-O-sulfated Arixtra. Thus, the catalytic residue E90 was selected for the mutagenesis and binding studies that is described in the following chapter.

CHAPTER 4

MUTAGENESIS AND BINDING ANALYSIS

In this chapter, site-directed mutagenesis and binding analysis of the 3-OST 1 wild type and mutants are covered. Four mutations (E90K, E90H, E90Q, and E90R) were introduced to the inactive sulfotransferase enzymes. The wild-type and mutant 3-OST 1 were expressed in the *E.coli* BL21(DE3) RIL expression system. The recombinant proteins were purified using Immobilized Metal Affinity Chromatography (IMAC) and Size Exclusion Chromatography (SEC) on the automated liquid chromatography system AKTA purifier. Binding analysis of 3-OST 1 WT and mutants towards different oligosaccharide substrates was examined by Bio-Layer Interferometry (BLI). The negatively charged glutamic acid residue was replaced by polar and positively charged residues, in order to alleviate the contribution of the carboxyl group to the repulsive interaction between the 3-OST 1 with the Arixtra.

4.1 MUTAGENESIS ANALYSIS

Site-directed mutagenesis(SDM) is a method to introduce specific changes in the double stranded plasmid DNA. SDM is used to study the structural and functional properties of the protein [60]. Custom designed oligonucleotide PCR primers are used to introduce point-mutations to the plasmid templates. Upon PCR amplification, the parent templates are removed by restriction digestion using the DpnI endonuclease and the mutagenized plasmids are transformed into E. coli BL21(DE3) for expression. A QuikChange mutagenesis kit (Stratagene)

was applied for the construction of E90 mutants. The bacterial expression plasmid (b3-OST-1-pET28) obtained from Dr. Jian Liu was used as template for the construction of mutant plasmids through PCR reaction.

4.2 BINDING ANALYSIS

In order to detect the affinity of the sulfotransferase mutants for the specific HS targets, binding analysis of 3-OST 1 was performed by BLI. Previously, binding analysis of HS and 3-OST 1 have been examined by Surface Plasmon Resonance (SPR), where biotinylated HS from bovine kidney were attached to the sensor chips [32,47]. However, HS chains have an heterogeneous structure that could contain a various number of receptor binding site. Therefore, in this study chemoenzymatically synthesized hexasaccharide HS fragments with defined sequence were used to examine the substrate specificity of the enzyme 3-OST 1 with HS.

The HS fragments were obtained from Dr. Jian Liu who has synthesized a wide range of oligosaccharides [3, 34]. For the binding and specificity characterizations, four HS hexasaccharides that displayed difference in the degree of sulfation was examined. The sequences of the hexasaccharides are presented in the table 3. Each one of the hexasaccharides contained either the substrate or product of 2-OST and 3-OST 1 enzymatic reaction. The reducing terminus of the HS fragment was conjugate to biotin. BLI was used to detect the affinity of the sulfotransferase mutants for the specific heparan sulfate target.

BLI is an optical analytical technique that measures the intermolecular interactions by examining the interference pattern of the white light reflected from the surface of the biosensor tip [35]. Similar to SPR, one of the biomolecule is immobilized on a sensor surface and the changes in the optical signals are detected to examine the association of the binding partner [36].

BLI signals are sensitive to the mass of the molecules that bind at the surface. Thus, in order to obtain a larger BLI signal, HS fragments that are relatively smaller (~2kDa) than the 3-OST 1 (33kDa) were chosen for immobilization on the biosensor surface. Since one of the binding partners are immobilized on the biosensor surface, mass transport limitations can affect the binding affinities and the binding constants [37]. In order to reduce the mass transport effect, the minimal level of the chemoenzymatically synthesized biotinylated HS fragments was loaded on the streptavidin coated biosensors (0.5 μg/mL) [35]. 3-OST 1 acted as the analyte. Multiple concentrations of the analyte were prepared in PBS buffer (50mM phosphate, 0.5M NaCl, pH 7.4) in order to determine robust rate of binding [36]. Single cycle binding analysis was performed to monitor the association of the 3-OST1 with the immobilized HS fragments. Binding kinetics of the WT and mutants were obtained by the equilibrium binding analysis.

	SEQUENCE OF THE HEXASACCHARIDE SEGMENT	NET CHARGE
substrate of 2-OST (sub2)	GlcNS-GlcA-GlcNS-IdoA-GlcNS-GlcA	6
product of 2-OST (prod2)	GlcNS-GlcA-GlcNS-IdoA2S-GlcNS-GlcA	7
substrate of 3-OST1 (sub3)	GlcNS6S-GlcA-GlcNS6S-IdoA2S-GlcNS6S-GlcA	10
product of 3-OST 1 (prod3)	GlcNS6S-GlcA-GlcNS6S3S-IdoA2S-GlcNS6S-GlcA	11

Table 3. THE BIOTINYLATED HS FRAGMENTS USED FOR BLI.

The chemoenzymatically synthesized HS fragments were obtained from Dr Jian Liu. For different HS fragments that displayed difference in the degree of sulfation (substrate of 2-OST activity, product of 2-OST activity, the substrate, and the product of 3-OST 1 activity) were submitted to BLI analysis. The binding analysis of the mutants for four ligand substrates were performed by immobilizing the HS fragments onto the biosensors.

4.3 MATERIAL AND METHODS

BACTERIAL EXPRESSION VECTOR

The bacterial expression plasmid (b3-OST-1-pET28) were obtained from Dr. Jian Liu (UNC Chapel Hill). The cDNA fragment encoding the catalytic domain of 3-OST 1 (G48-H311) from *Mus musculus* was ligated into the pET 28a expression vector using a 5' overhang containing an NdeI site and a 3' overhang containing an EcoRI site. The bacterial expression plasmid (b3-OST-1-pET28) also contained the T7lac promoter in the upstream region of the coding sequence for the controlled expression of recombinant protein. 3-OST 1 protein contained an N-terminal hexyl histidine tag. The bacterial plasmid was transformed into the BL21(DE3) RIPL cells.

PROTEIN EXPRESSION AND PURIFICATION

The expression of 3-OST 1 was performed in E*scherichia coli* using BL21 cells. The glycerol stock containing the transformed cells were grown in 5mL LB medium that contained 50μg/ml kanamycin in a shaking incubator at 37 ℃ overnight. The inoculated 5mL culture then was used to grow 1 liter of LB media containing 50μg/ml kanamycin in 2.8-liter Fernbach flasks at 37 ℃. When the A_{600} reached 0.6-0.8, the temperature was lowered to 22 ℃ for 15 min. Then the isopropyl-β-D-thiogalactopyranoside (IPTG) was added to a final concentration of 200μM, and the second inducer was added after an additional 20 min. The cells were allowed to grow in the shaking incubator overnight at 22 ℃. Next morning, the cells were harvested by centrifugation at 6000 rpm for 30 min. Then the cell pellet was collected resuspended in 120mL of sonication/binding buffer containing 25mM Tris, pH7.5, 500mM NaCl, and 30mM imidazole. Cells were disrupted by sonication then spun down at 12500 rpm for 30 min in order to obtain

the supernatant that contained the soluble fraction. Before the suspension was loaded onto the IMAC column, the supernatant was filtered through a 0.45μm filter.

During the Immobilized Metal Ion Affinity Chromatography (IMAC), the His-Trap HP (GE Healthcare) columns that was prepacked with nickel sepharose was washed with 25mL of sonication/binding buffer. Then the supernatant was loaded onto the column and eluted in 20mL of the elution buffer containing 25mM Tris, pH7.5, 500mM NaCl, and 300mM imidazole. The obtained fractions were concentrated using a centrifugal filter (10kDa cutoff). The IMAC purified fractions were concentrated to 500μL and submitted to SEC chromatography using Superose 12 10/300 high performance columns (GE Healthcare). The concentration of the obtained proteins were measured by the spectrophotometer. The obtained elution fractions were analyzed by denaturing SDS-PAGE.

MUTANT EXPRESSION AND PURIFICATION

E90 mutants (E90K/ E90R/E90H/ E90Q) were generated using the b3-OST1-pET28 as the template. The PureLink Quick Miniprep Kit (Invitrogen) was used to isolate the WT plasmid DNA. Then point mutation was introduced to the catalytic residue using the Agilent's QuikChangeTM Lightning site-directed mutagenesis kit. The length and the sequences of the primers for preparation of those mutants were designed based on the manufacturer's protocol for this mutagenesis kit and were synthesized by Intergrated DNA Technologies (ITD). The resultant plasmids were sequenced to confirm the reading frame and the mutations within the coding region (University of Georgia, Georgia Genomics and Bioinformatics Core). The expression plasmids for various 3-OST 1 mutants were transformed individually into BL21(DE3)

RIL cells. Each of the mutants that contained the histidine-tag were expressed and purified as for the wild-type of 3-OST 1.

BINDING ASSAYS

Binding analysis of 3-OST 1 towards different oligosaccharide substrates was examined by Bio-Layer Interferometry (BLI) using the OCTET RED96 system. Four chemoenzymatically synthesized HS fragments that displayed difference in the degree of sulfation were incorporated in the study in order to examine if the substrate specificity of the enzyme 3-OST 1; sub 2 (GlcNS-GlcA-GlcNS-IdoA-GlcNS-GlcA-pA-PEG4-Biotin), prod 2 (GlcNS-GlcA-GlcNS-IdoA2S-GlcNS-GlcA-pA-PEG4-Biotin-), sub 3 (GlcNS6S-GlcA-GlcNS6S-IdoA2S-GlcNS6S-GlcA- pA-PEG4-Biotin-), and prod 4 (GlcNS6S-GlcA-GlcNS6S3S-IdoA2S-GlcNS6S-GlcA-pA-PEG4-Biotin-).

The HS hexasaccharide fragments were immobilized onto streptavidin biosensors using the lowest practical loading density (0.5μg/mL) for the accurate K_D measurement [35]. In order to minimize the mass transport related effect multiple concentrations of the analyte were prepared in phosphate-buffered saline (PBS, pH 7.4) from 4μM (132μg/mL) to 0.008 μM (0.261μg/mL). Two-fold serial dilutions of the enzyme at a volume of 250 μL per well was prepared. One vertical column of wells contained only buffer, which served as reference samples. In order to account for the non-specific interactions, the binding of the protein to the bare biosensor (no glycan immobilized on the biosensor) was also measured. The protein samples were loaded on the 96-well plates that was agitated by the rocking platform.

Prior to the binding measurements, the streptavidin biosensors were pre-hydrated. Then the sensor tips were transferred to the wells containing HS fragment for the loading step. The

binding interactions were measured by placing the HS-coated biosensors into the wells containing 3-OST 1 at various concentrations. The single cycle binding analysis of the 3-OST 1 was monitored through the consecutive 420-sec association steps.

4.5 RESULTS AND DISCUSSION

The successful purification of the wild-type and mutant was achieved by optimizing the induction, sonication, buffer, and purification conditions. During the IMAC purification, a single 100% elution wash (300mM imidazole) was performed. The obtained IMAC purification samples displayed a high level of non-specific proteins in the SDS-PAGE gels. Thus, the fractions were concentrated and submitted to size exclusion column to separate the proteins based on the molecular weight. SEC purification improved the purity of the purified proteins; the SDS PAGE gels showed that the non-specific proteins were separated from the 33kDa protein band that corresponds to the molecular weight of 3-OST 1. The IMAC sensograms, SEC sensograms, and the SDS-PAGE gels of the 3-OST 1 WT and mutants are provided in the appendix.

The concentrations of the protein samples were measured by spectrophotometry; the obtained protein yield of the 1L LB culture of 3-OST 1 WT is ~0.46mg (~0.28mg from fraction 11 and ~0.18mg from fraction 12). The total protein yield of the 3-OST 1 mutants from the 1 L LB culture was ~0.74 mg for E90K (~ 0.43 mg from fraction 11 and ~ 0.31 mg from fraction 12), ~0.67 mg for E90H (~ 0.36 mg from fraction 10 and ~0.31 mg from fraction 11), ~0.46 mg for E90R (~ 0.24 mg for fraction 12 and ~ 0.22 mg for fraction 13), and ~ 0.49 mg for E90Q (~ 0.21 mg for fraction 11 and ~ 0.28mg from the fraction 12).

The purified protein samples were then submitted to binding analysis using BLI. The raw data was analyzed by the Octet Data Analysis software. The sensor's signals were referenced using a parallel buffer blank subtraction and the baseline was aligned to the y-axis by the Savitzky-Goaly filtering function of the data analysis software. The disassociation constants were obtained by fitting the obtained equilibrium binding analysis data to a 1:1 Langmuir binding model using Prism software (version 7.03, GraphPad Software, La Jolla, USA). The sensograms and the obtained raw data are presented in the appendix. The obtained K_D values are presented in the table 4.

K_D (μM)				
	Sub2	Prod2	Sub3	Prod3
WT	1.11	1.79	0.49	0.47
E90H	1.12	2.60	0.47	0.16
E90Q	0.34	0.50	0.32	0.25
E90R	0.09	0.21	0.10	0.08
E90K	0.35	0.59	0.36	0.11
RELATIVE AFFINITY ENHANCEMENT RELATIVE TO 3-OST1 WT				
	Sub2	Prod2	Sub3	Prod3
WT	1.0	1.0	1.0	1.0
E90H	1.0	0.7	1.0	2.9
E90Q	3.3	3.6	1.6	1.8
E90R	11.8	8.6	4.8	5.9
E90K	3.2	3.0	1.4	4.2

TABLE 4: BIO-LAYER INTERFEROMETRY BINDING DATA FOR 3-OST 1.

K_D values for the interaction between the 3-OST 1 with the HS fragments at determined by BLI. The biotinylated HS fragments were immobilized on the streptavidin biosensors and 3-OST 1 was the analyte. K_D values were obtained from the 1:1 Langmuir binding model

Overall the mutants displayed a small enhancement in the affinity relative to the wild type for HS fragments. When the negative carboxyl group was removed in the E90Q mutant, the relative affinity improved by 2~3 folds. The affinity enhancement could be contributed to the removal of the repulsive charge-to-charge interaction between the carboxyl group and the sulfate groups of the HS. The binding affinity of the E90H mutant was not affected significantly, since the imidazole group of the E90H side chain was deprotonated during the experiment; the analytes were prepared in PBS (pH 7.4). In order to examine the contribution of the functional group of the histidine residue, the affinity should be measured in lower pH conditions. In E90R, when the carboxyl group was replaced by the guanidine side chain, the E90R mutant displayed the highest increase in the affinity towards the HS (up to 11.8-fold enhancement of the binding affinity). The E90K residues also displayed an increase in the binding affinity. Overall, the introduction of the positive charge to the catalytic residue enhanced the binding affinities.

In order to screen 3-OST 1 mutants for their ability to bind specific sulfation patterns, binding analysis of 3-OST 1 towards different oligosaccharide substrates was examined. The results of the BLI analysis overall showed that the mutants displayed enhanced affinity for the Sub3 and Prod3 that contained more sulfo groups; the affinity increase was proportional to the negative charge of the HS fragments. The additional sulfate group of the Sub3 and Prod3 enhanced the binding affinity of the enzyme-ligand complex in the binding site, since they interact with the polar and positively charged amino acid residues [32,47]. The substrate and product of 3OST-1 that had a similar net charge, displayed similar K_D values.

According to the structural analysis of the 3-OST 1 and Arixtra, the catalytic residue interacts with the negatively charged carboxyl group of the linked GlcA residue, 3S of the

acceptor GlcNS3, and the NS of the acceptor GlcNS3S6S. The carboxyl group of the linked GlcA residue and the NS of the acceptor GlcNS6S were consistently present within the four chemoenzymatically synthesized substrate. In order to investigate the substrate specificity of 3-OST 1 mutants towards specific HS fragments, further analysis that incorporate different HS sequences should be performed.

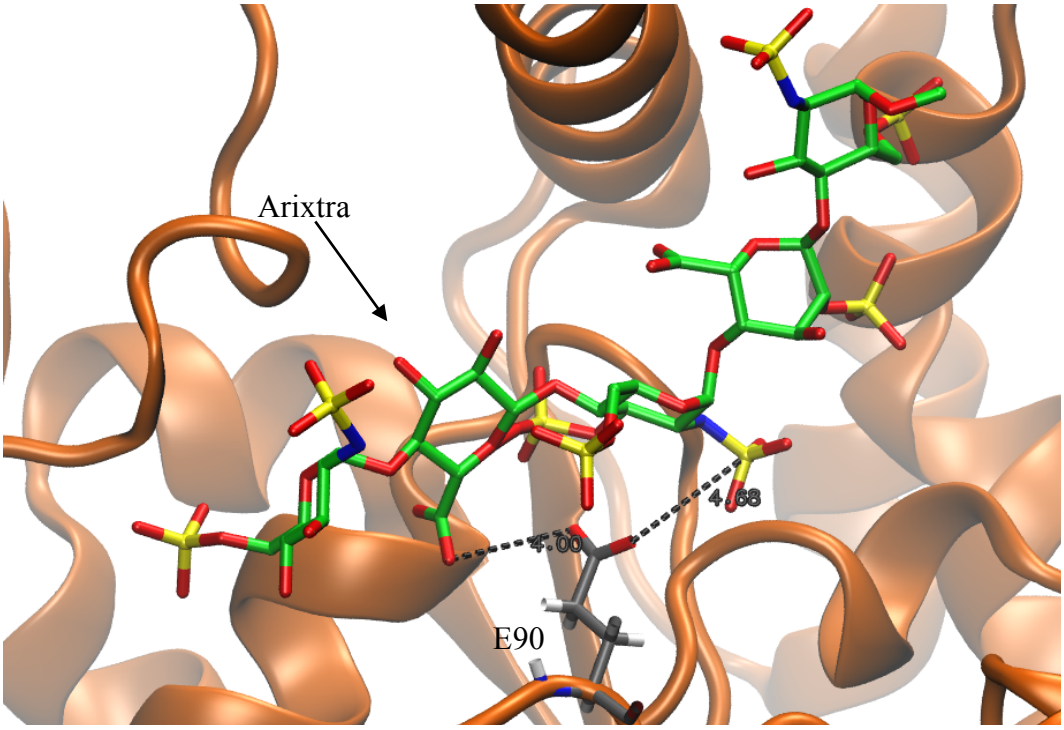

FIGURE 10. POSITION OF E90 RELATIVE TO ARIXTRA

Position of E90 in relation to the N-sulfated position of glucosamine and the carboxyl group of the glucuronic acid of the substrate. The catalytic residue may interact with the negatively charged moieties of Arixtra. Snapshot image from the MD simulation of 3-OST 1 and Arixtra complex

CHAPTER 5

CONCLUSIONS

The goal of this project was to develop a reagent that would target a specific sulfation patterns of HS from a catalytically inactive sulfotransferase. Thus, the substrate specificity of the enzyme 3-O-sulfotransferase isoform 1 (3-OST 1) that is involved in the last step of the HS biosynthetic pathway was exploited. The inherent specificity of the enzyme was exploited for the development of high-affinity reagent that would target the product of the 3-OST 1 enzymatic reaction, the anticoagulant HS.

Molecular dynamics (MD) simulations and MM-GBSA analysis were performed to examine the structure and the free energy between 3-OST 1 and the 3-O-sulfated HS. MD simulation and MM-GBSA analysis showed that the catalytic residue is the most unfavorable to the binding interaction. The carboxyl group of E90 was theorized to have a repulsive effect on the binding of the protein to a 3-OST 1 modified HS fragment. Thereby, in order to convert the 3-OST 1 into high-affinity binding probe, site-directed mutagenesis was performed on the catalytic glutamic acid (E90) residue and the effects of the mutations in binding to HS fragments were investigated by Bio-Layer Interferometry (BLI) analysis.

The polar and positively charged E90 mutants were expected to enhance the binding affinities of the complex. The results of the BLI analysis overall showed a modest enhancement in the affinity relative to the wild type for HS fragments. The introduction of a positively charged

residue in the catalytic site increased the affinity for the HS fragment proportionally to the negative charge of the HS fragment.

The mutagenesis and binding analysis demonstrate that the substrate affinity cannot be enhance by a single mutation of the 3-OST 1. MM-GBSA analysis has identified a number of residues that are unfavorable for the binding interaction between the 3-OST 1 and the 3-O-sulfated HS fragment; E76, E88, D95 and D160 residues could also be submitted to mutagenesis studies to enhance the affinity of the catalytically-inactive enzymes towards the anticoagulant HS.

REFERENCES

1. Gandhi NS, Mancera RL. The structure of glycosaminoglycans and their interaction with proteins. Chem Biol Drug Des. 2008;72:455–482
2. Bishop JR, Schuksz M, Esko JD. Heparan sulphate proteoglycans fine-tune mammalian physiology. Nature. 2007. 446: 1030–1037
3. Sarkar A, Desai UR. A Simple Method for Discovering Druggable, Specific Glycosaminoglycan-Protein Systems. Elucidation of Key Principles from Heparin/Heparan Sulfate-Binding Proteins. PLoS One. 2015. 10; (10)
4. Wang Z, Hsieh PH, Xu Y, Thieker D, Chai EJ, Xie S, Cooley B, Woods RJ, Chi L, Liu J. Synthesis of 3-O-sulfated oligosaccharides to understand the relationship between structures and functions of heparan sulfate. Journal of the American Chemical Society. 2017 Apr 3;139(14):5249-56.
5. Mulloy B, Linhardt RJ. *Order out of complexity – protein structures that interact with heparin*. Curr Opin Struct Biol . 2001; 5; 623-628.
6. Tkachenko E, Rhodes JM, Simons M. Syndecans: New kids on the signaling block. Circ Res. 2005. 96: 488–500
7. Bulow HE, Hobert O 2006. The molecular diversity of glycosaminoglycans shapes animal development. Annu Rev Cell Dev Biol 22: 375–407
8. Sugahara K, Kitagawa H. Heparin and heparan sulfate biosynthesis. *IUBMB Life* 2002. 54:163– 75
9. Sanderson RD, Yang Y. Syndecan-1: A dynamic regulator of the myeloma microenvironment. Clin Exp Metastasis. 2008. 25: 149–159
10. Sarrazin S, Lamanna WC, Esko JD. Heparan sulfate proteoglycans. Cold Spring Harb Perspect Biol. 2011 Jul 1;3(7)
11. Imberty A, Lortat-Jacob H, Perez S. Structural view of glycosaminoglycan–protein interactions. Carbohydr Res. 2007; 342:430–439
12. Shriver Z, Capila I, Venkataraman G, Sasisekharan R. Heparin and Heparan Sulfate: Analyzing Structure and Microheterogeneity. *Handbook of experimental pharmacology*. 2012;(207):159-176
13. Canales A, Angulo J, Ojeda R, Bruix M, Fayos R, Lozano R, Gimenez-Gallego G, Martin-Lomas M, Nieto PM, Jimenez-Barbero J. Conformational flexibility of a synthetic glycosylaminoglycan bound to a fibroblast growth factor. FGF-1 recognizes both the (1)C(4) and (2)S(O) conformations of a bioactive heparin-like hexasaccharide. *J Am Chem Soc.* 2005; 127:5778–5779.
14. Xu D, Esko JD. Demystifying heparan sulfate-protein interactions. Annu Rev Biochem. 2014; 83:129-57
15. Weiss RJ, Esko JD, Tor Y. Targeting heparin and heparan sulfate protein interactions. *Org. Biomol. Chem.* 2017 ;15: 5656-5668
16. Muñoz EM, Linhardt RJ. Heparin-Binding Domains in Vascular Biology. *Arteriosclerosis, thrombosis, and vascular biology*. 2004;24(9):1549-1557.

17. Esko JD, Linhardt RJ. Proteins that Bind Sulfated Glycosaminoglycans. In: Varki A, Cummings RD, Esko JD, et al., editors. Essentials of Glycobiology. 2nd edition. Cold Spring Harbor (NY): Cold Spring Harbor Laboratory Press; 2009. Chapter 35. Available from: https://www.ncbi.nlm.nih.gov/books/NBK1948/
18. Pichert A, Samsonov SA, Theisgen S, et al. Characterization of the interaction of interleukin-8 with hyaluronan, chondroitin sulfate, dermatan sulfate and their sulfated derivatives by spectroscopy and molecular modeling. *Glycobiology*. 2012;22(1):134-145
19. Borza DB., Morgan WT. Histidine–proline-rich glycopro- tein as a plasma pH sensor. Modulation of its interaction with glycosaminoglycans by pH and metals. J Biol Chem. 1998;273:5493– 5499.
20. Singh A, Kett WC, Severin IC, et al. The Interaction of Heparin Tetrasaccharides with Chemokine CCL5 Is Modulated by Sulfation Pattern and pH. *The Journal of Biological Chemistry*. 2015;290(25):15421-15436.
21. Trott O, Olson AJ. AutoDock Vina: improving the speed and accuracy of docking with a new scoring function, efficient optimization and multithreading. *Journal of computational chemistry*. 2010;31(2):455-461.
22. Stewart KL, Hughes E, Yates EA, Akien GR, Huang TY, Lima MA, Rudd TR, Guerrini M, Hung SC, Radford SE, Middleton DA. Atomic details of the interactions of glycosaminoglycans with amyloid-β fibrils. J. Am. Chem. Soc. 2016 Jul 5;138(27):8328-31.
23. Kim SY, Zhao J, Liu X, Fraser K, Lin L, Zhang X., ... & Linhardt RJ. Interaction of Zika virus envelope protein with glycosaminoglycans. *Biochemistry*. 2017. *56*(8), 1151-1162.
24. Takaoka T, Mori K, Okimoto N, Neya S, Hoshino T. Prediction of the structure of complexes comprised of proteins and glycosaminoglycans using docking simulation and cluster analysis. J Chem Theory Comput. 2007. 3:2347–2356.
25. Hileman RE, Fromm JR, Weiler JM, Linhardt RJ. Glycosaminoglycan-protein interactions: definition of consensus sites in glycosaminoglycan binding proteins. Bioessays. 1998 Feb; 20(2):156-67.
26. Moon AF, Xu Y, Woody SM, et al. Dissecting the substrate recognition of 3-*O*-sulfotransferase for the biosynthesis of anticoagulant heparin. *Proceedings of the National Academy of Sciences of the United States of America*. 2012;109(14):5265-5270. doi:10.1073/pnas.1117923109.
27. Tessier MB, Grant OC, Heimburg-Molinaro J, Smith D, Jadey S, Gulick AM, Glushka J, Deutscher SL, Rittenhouse-Olson K, Woods RJ. Computational screening of the human TF-glycome provides a structural definition for the specificity of anti-tumor antibody JAA-F11. PLoS One. 2013 Jan 24;8(1)
28. Van Den Born J, Salmivirta K, Henttinen T, Östman N, Ishimaru T, Miyaura S, Yoshida K, Salmivirta M. Novel heparan sulfate structures revealed by monoclonal antibodies. Journal of Biological Chemistry. 2005 May 27;280(21):20516-23.
29. Angulo J, Nieto PM. STD-NMR: application to transient interactions between biomolecules—a quantitative approach. European Biophysics Journal. 2011 Dec 1;40(12):1357-69.
30. Sapay N, Cabannes E, Petitou M, Imberty A. Molecular modeling of the interaction between heparan sulfate and cellular growth factors: bringing pieces together. Glycobiology. 2011 May 13;21(9):1181-93.
31. Place ES, Evans ND, Stevens MM. Complexity in biomaterials for tissue engineering. Nature materials. 2009 Jun 1;8(6):457.

32. Edavettal SC, Lee KA, Negishi M, Linhardt RJ, Liu J, Pedersen LC. Crystal structure and mutational analysis of heparan sulfate 3-O-sulfotransferase isoform 1. J Biol Chem. 2004; 279: 25789–97.
33. Moon AF, Edavettal SC, Krahn JM, Munoz EM, Negishi M, Linhardt RJ, Liu J, Pedersen LC. Structural analysis of the sulfotransferase (3-o-sulfotransferase isoform 3) involved in the biosynthesis of an entry receptor for herpes simplex virus 1. Journal of Biological Chemistry. 2004 Oct 22;279(43):45185-93.
34. Liu J, Moon AF, Sheng J, Pedersen LC. Understanding the substrate specificity of the heparan sulfate sulfotransferases by an integrated biosynthetic and crystallographic approach. Current opinion in structural biology. 2012 Oct 31;22(5):550-7.
35. Estep P, Reid F, Nauman C, Liu Y, Sun T, Sun J, Xu Y. High throughput solution-based measurement of antibody-antigen affinity and epitope binning. InMAbs 2013 Mar 1 (Vol. 5, No. 2, pp. 270-278).
36. Shah NB, Duncan TM. Bio-layer interferometry for measuring kinetics of protein-protein interactions and allosteric ligand effects. Journal of visualized experiments: JoVE. 2014(84).
37. Abdiche Y, Malashock D, Pinkerton A, Pons J. Determining kinetics and affinities of protein interactions using a parallel real-time label-free biosensor, the Octet. Analytical biochemistry. 2008 Jun 15;377(2):209-17.
38. Wagstaff JL, Taylor SL, Howard MJ. Recent developments and applications of saturation transfer difference nuclear magnetic resonance (STD NMR) spectroscopy. Molecular BioSystems. 2013;9(4):571-7.
39. Cala O, Guillière F, Krimm I. NMR-based analysis of protein–ligand interactions. Analytical and bioanalytical chemistry. 2014 Feb 1;406(4):943-56.
40. Meyer B, Klein J, Mayer M, Meinecke R, Möller H, Neffe A, Schuster O, Wülfken J, Ding Y, Knaie O, Labbe J. Saturation transfer difference NMR spectroscopy for identifying ligand epitopes and binding specificities. InLeucocyte trafficking 2004 (pp. 149-167). Springer, Berlin, Heidelberg.
41. Huo S, Massova I, Kollman PA. Computational alanine scanning of the 1: 1 human growth hormone–receptor complex. Journal of computational chemistry. 2002 Jan 15;23(1):15-27.
42. Lindahl U, Li JP. Interactions between heparan sulfate and proteins—design and functional implications. International review of cell and molecular biology. 2009 Dec 31;276:105-59.
43. Sarrazin S, Lamanna WC, Esko JD. Heparan Sulfate Proteoglycans. Cold Spring Harbor Perspectives in Biology. 2011 Jun 20:a004952.
44. Rabenstein DL. Heparin and heparan sulfate: structure and function. Natural product reports. 2002;19(3):312-31.
45. Fadda E, Woods RJ. Molecular simulations of carbohydrates and protein–carbohydrate interactions: motivation, issues and prospects. Drug discovery today. 2010 Aug 31; 15(15): 596-609.
46. Dror RO, Dirks RM, Grossman JP, Xu H, Shaw DE. Biomolecular simulation: a computational microscope for molecular biology. Annual review of biophysics. 2012 Jun 9;41:429-52.
47. Muñoz E, Xu D, Kemp M, Zhang F, Liu J, Linhardt RJ. Affinity, kinetic, and structural study of the interaction of 3-O-sulfotransferase isoform 1 with heparan sulfate. Biochemistry. 2006 Apr 25;45(16):5122-8.
48. Groenhof G. Introduction to QM/MM simulations. Biomolecular simulations: methods and protocols. 2013:43-66.

49. Kirschner KN, Yongye AB, Tschampel SM, González-Outeiriño J, Daniels CR, Foley BL, Woods RJ. GLYCAM06: a generalizable biomolecular force field. Carbohydrates. Journal of computational chemistry. 2008 Mar 1;29(4):622-55.
50. Case DA, Cheatham TE, Darden T, Gohlke H, Luo R, Merz KM, Onufriev A, Simmerling C, Wang B, Woods RJ. The Amber biomolecular simulation programs. Journal of computational chemistry. 2005 Dec 1;26(16):1668-88.
51. Chen F, Liu H, Sun H, Pan P, Li Y, Li D, Hou T. Assessing the performance of the MM/PBSA and MM/GBSA methods. 6. Capability to predict protein–protein binding free energies and re-rank binding poses generated by protein–protein docking. Physical Chemistry Chemical Physics. 2016;18(32):22129-39.
52. Frenzel D, Willbold D. Kinetic titration series with biolayer interferometry. PloS one. 2014 Sep 17;9(9):e106882.
53. Kshirsagar S, Mandadapu KK, Papadopoulos P. Classical molecular dynamics simulations of crystal lattices with truncated Taylor series-based interatomic potentials. Computational Materials Science. 2016 Jul 31;120:127-34
54. Eaton BE, Gold L, Zichi DA. Let's get specific: the relationship between specificity and affinity. Chemistry & biology. 1995 Oct 31;2(10):633-8.
55. Chu X, Wang J. Specificity and affinity quantification of flexible recognition from underlying energy landscape topography. PLoS computational biology. 2014 Aug 21;10(8):e1003782.
56. Case DA, Darden TA, Cheatham III TE, Simmerling CL, Wang J, Duke RE, Luo R, Crowley MR, Walker RC, Zhang W, Merz KM. AMBER 10; University of California: San Francisco, 2008. There is no corresponding record for this reference. 2005.
57. Hornak V, Abel R, Okur A, Strockbine B, Roitberg A, Simmerling C. Comparison of multiple Amber force fields and development of improved protein backbone parameters. Proteins: Structure, Function, and Bioinformatics. 2006 Nov 15;65(3):712-25.
58. Kollman PA, Massova I, Reyes C, Kuhn B, Huo S, Chong L, Lee M, Lee T, Duan Y, Wang W, Donini O. Calculating structures and free energies of complex molecules: combining molecular mechanics and continuum models. Accounts of chemical research. 2000 Dec 19;33(12):889-97.
59. Onufriev A, Bashford D, Case DA. Exploring protein native states and large-scale conformational changes with a modified generalized born model. Proteins: Structure, Function, and Bioinformatics. 2004 May 1;55(2):383-94.
60. Liu H, Naismith JH. An efficient one-step site-directed deletion, insertion, single and multiple-site plasmid mutagenesis protocol. BMC biotechnology. 2008 Dec 4;8(1):91.

APPENDICES

APPENDIX A

BUFFER CONDITIONS

PROTEIN EXPRESSION MEDIA

Bactor Agar (3.2% tryptone, 2% yeast extract, and 0.5% NaCl)

SONICATION BUFFER

25mM Tris, 500mM NaCl, 30mM Imidazole, pH 7.4

ELUTION BUFFER

25mM Tris, 500mM NaCl, 300mM Imidazole, pH 7.4

PHOSPHATE-BUFFERED SALINE (PBS, PH 7.4)

As per manufacturer 1x PBS was prepared using the 10X PBS (Biorad)

APPENDIX B

SITE DIRECTED MUTAGENESIS PRIMERS

PRIMER TYPTE	SEQEUNCE	MELTING TEMPERUATURE (Tm)	G+C CONTENTS (%)
E90K FORWARD	GCTGCAGCTGAAAACAAAGTCCATTTCTTTGAC	78.4 ℃	42.4
E90K REVERSE	GTCAAAGAAATGGACTTTGTTTTCAGCTGCAGC	78.4 ℃	42.4
E90H FORWARD	GCTGCAGCTGAAAACCATGTCCATTTCTTTGAC	79.7 ℃	45.5
E90H REVERSE	GTCAAAGAAATGGACATGGTTTTCAGCTGCAGC	79.7 ℃	45.5
E90Q FORWARD	GCTGCAGCTGAAAACCAAGTCCATTTCTTTGAC	79.7 ℃	45.5
E90Q REVERSE	GTCAAAGAAATGGACTTGGTTTTCAGCTGCAGC	79.7 ℃	45.5
E90R FORWARD	GCTGCAGCTGAAAACCGGGTCCATTTCTTTGAC	82.2 ℃	51.5
E90R REVERSE	GTCAAAGAAATGGACCCGGTTTTCAGCTGCAGC	82.2 ℃	51.5

Table 5. SITE DIRECTED MUTAGENESIS PRIMERS

The mutagenic oligonucleotide primers were designed according to the manufacture's guidelines. Each primer contained 33 bases in length. The desired mutation was in the middle of the primer with 15 bases on both sides. Each of the primer's melting temperature (Tm) was ≥78°C. The equation used for the melting temperature is Tm= 81.5 + 0.41(%G+C) - 675/N, where N= total number of the bases.

APPENDIX C

MUTANT PLASMID SEQUENCING

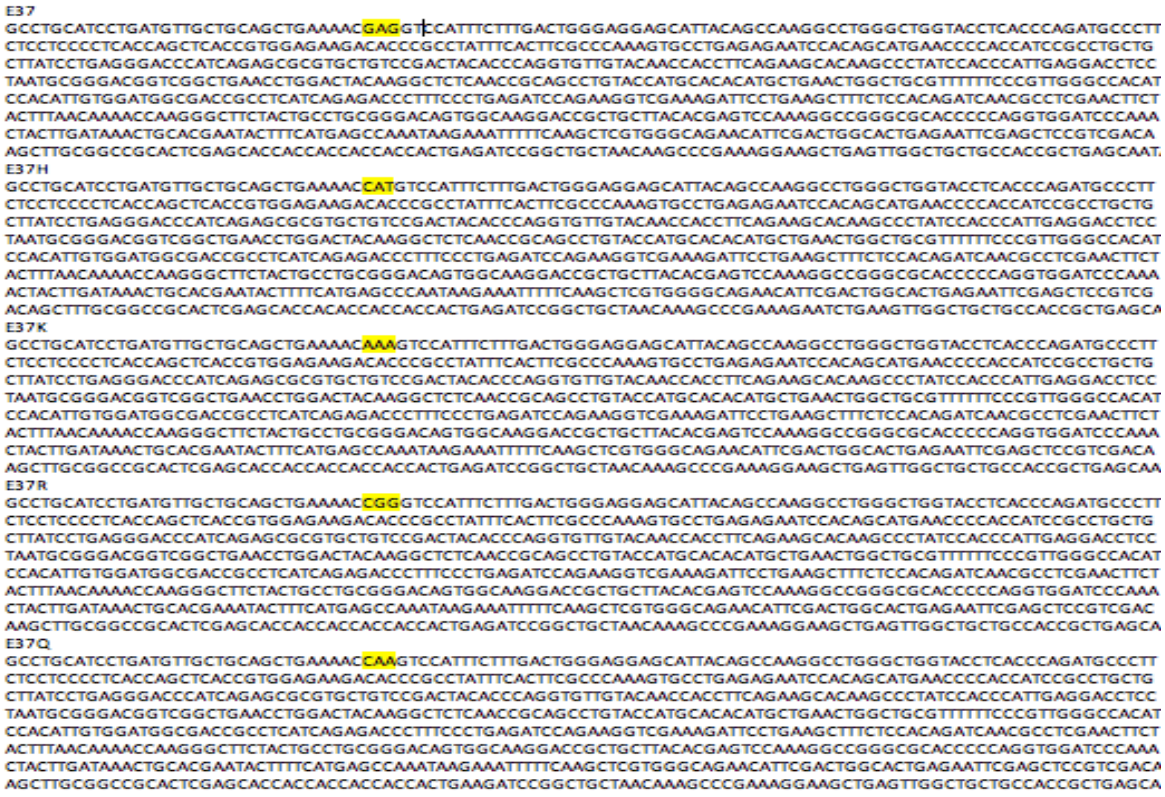

Figure 11. MUTANT PLASMID SEQUENCING.

Once the site-directed mutagenesis was performed to verify if the mutagenesis had been performed correctly, the obtained plasmids were sequenced at the Georgia Genomics and Bioinformatics Core. The nucleotide sequences that are found at the mutation site are highlighted in yellow. In the 3-OST 1 the codon GAG that corresponds to glutamic acid was present. In the E90H mutant, the GAG codon was replaced by the CAT codon that corresponds to the histidine residue. In the E90K mutant, the GAG codon was replaced by the CAA codon that corresponds to the lysine residue. In the E90R mutant, the GAG codon was replaced by the CGG codon that corresponds to the arginine residue. In the E90Q mutant, the GAG codon was replaced by the CAA codon that corresponds to the glutamine residue.

APPENDIX D

IMAC AND SEC ELUTION CHROMATOGRAMS

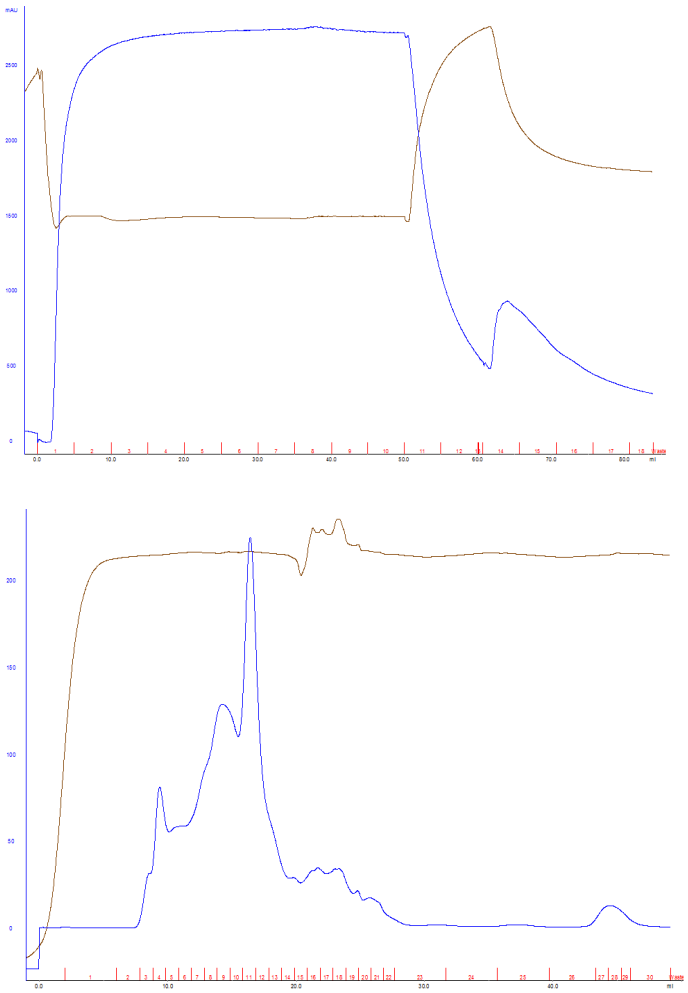

FIGURE 12. IMAC AND SEC ELUTION CHROMATOGRAM OF 3-OST 1 WT.

IMAC elution chromatogram (top). The bound protein was eluted with 100% IMAC B (fractions 14~18). The elution fractions were combined and concentrated for SEC chromatography.

SEC chromatogram on a superose 12 10/300 column (bottom). IMAC elution fractions were loaded on SEC column. The peak collected in fractions 11 and 12 contained a 33kDa band (based on SDS-PAGE shown in Figure 17). The blue traces indicate the UV absorption and orange traces indicate the conductivity readings that were recorded during the chromatography assays.

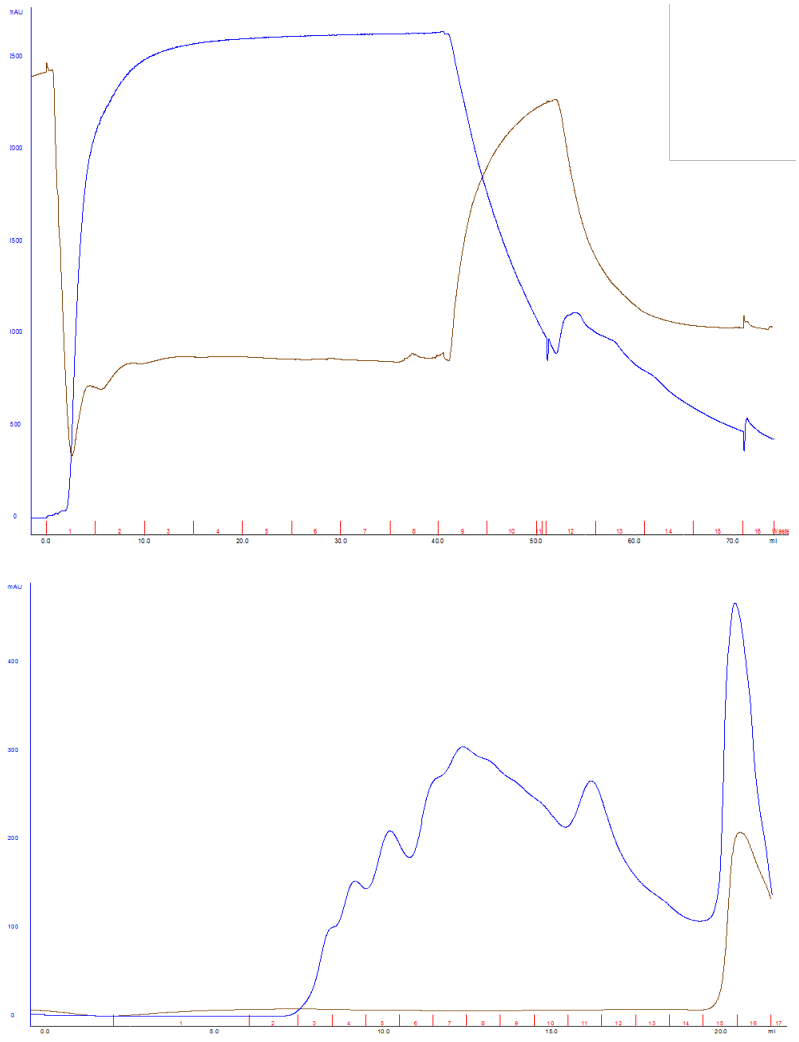

FIGURE 13. IMAC AND SEC ELUTION CHROMATOGRAM OF 3-OST 1 E90K.

IMAC elution chromatogram (top). The bound protein was eluted with 100% IMAC B (fractions 12~16). The elution fractions were combined and concentrated for SEC chromatography.

SEC chromatogram on a superose 12 10/300 column (bottom). IMAC elution fractions were loaded on SEC column. The peak collected in fractions 11 and 12 contained a 33kDa band (based on SDS-PAGE shown in Figure 18). The blue traces indicate the UV absorption and orange traces indicate the conductivity readings that were recorded during the chromatography assays.

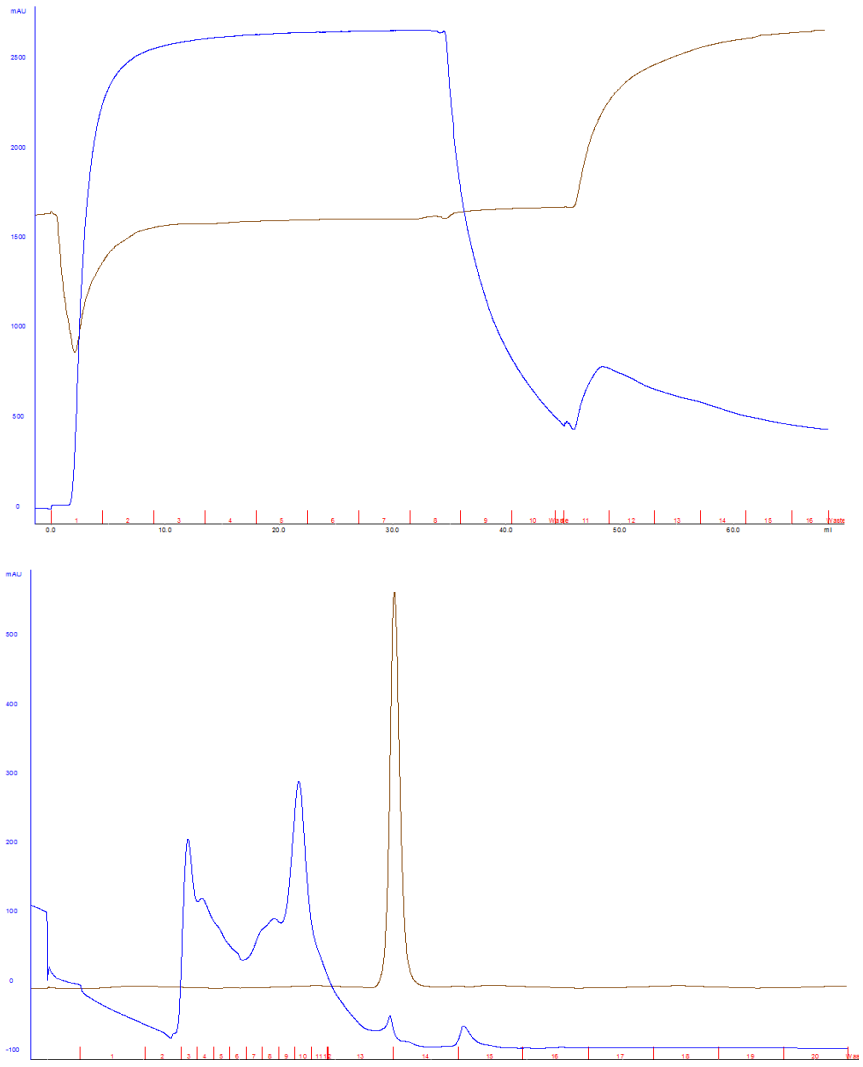

FIGURE 14. IMAC AND SEC ELUTION CHROMATOGRAM OF 3-OST 1 E90H.

IMAC elution chromatogram (top). The bound protein was eluted with 100% IMAC B (fractions 11~16). The elution fractions were combined and concentrated for SEC chromatography.

SEC chromatogram on a superose 12 10/300 column (bottom). IMAC elution fractions were loaded on SEC column. The peak collected in fractions 10 and 11 contained a 33kDa band (based on SDS-PAGE shown in Figure 19). The blue traces indicate the UV absorption and orange traces indicate the conductivity readings that were recorded during the chromatography assays.

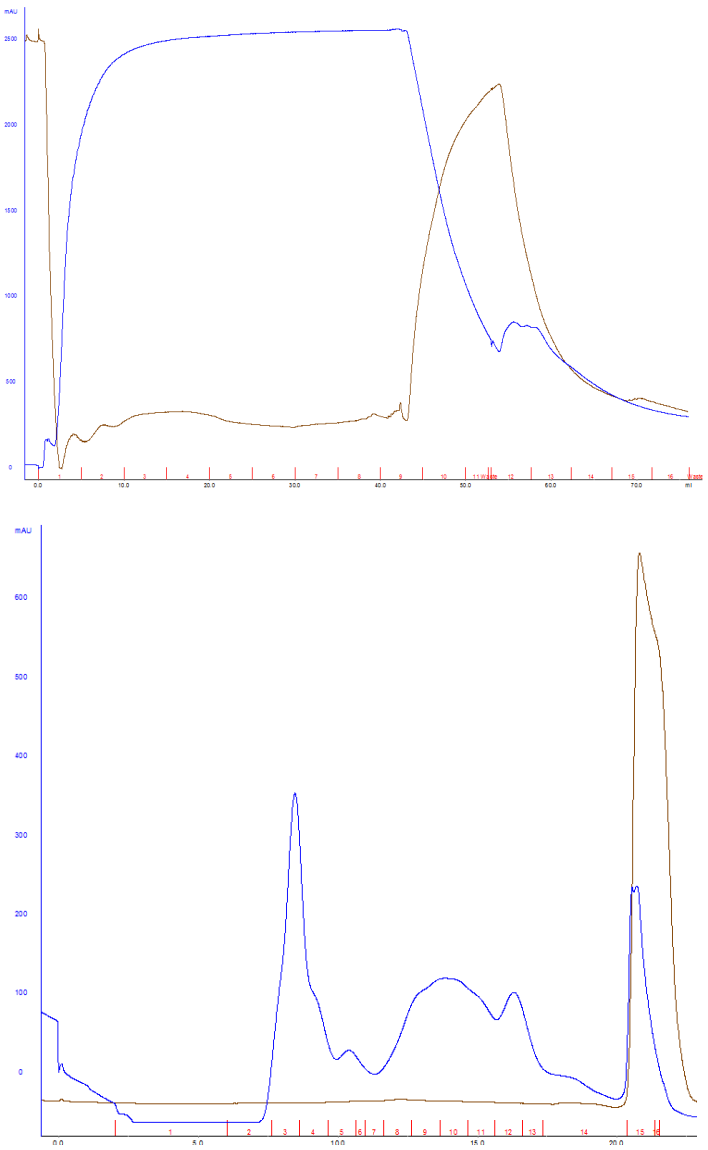

FIGURE 15. IMAC AND SEC ELUTION CHROMATOGRAM OF 3-OST 1 E90R.

IMAC elution chromatogram (top). The bound protein was eluted with 100% IMAC B (fractions 12~16). The elution fractions were combined and concentrated for SEC chromatography.

SEC chromatogram on a superose 12 10/300 column (bottom). IMAC elution fractions were loaded on SEC column. The peak collected in fractions 12 and 13 contained a 33kDa band (based on SDS-PAGE shown in Figure 20). The blue traces indicate the UV absorption and orange traces indicate the conductivity readings that were recorded during the chromatography assays.

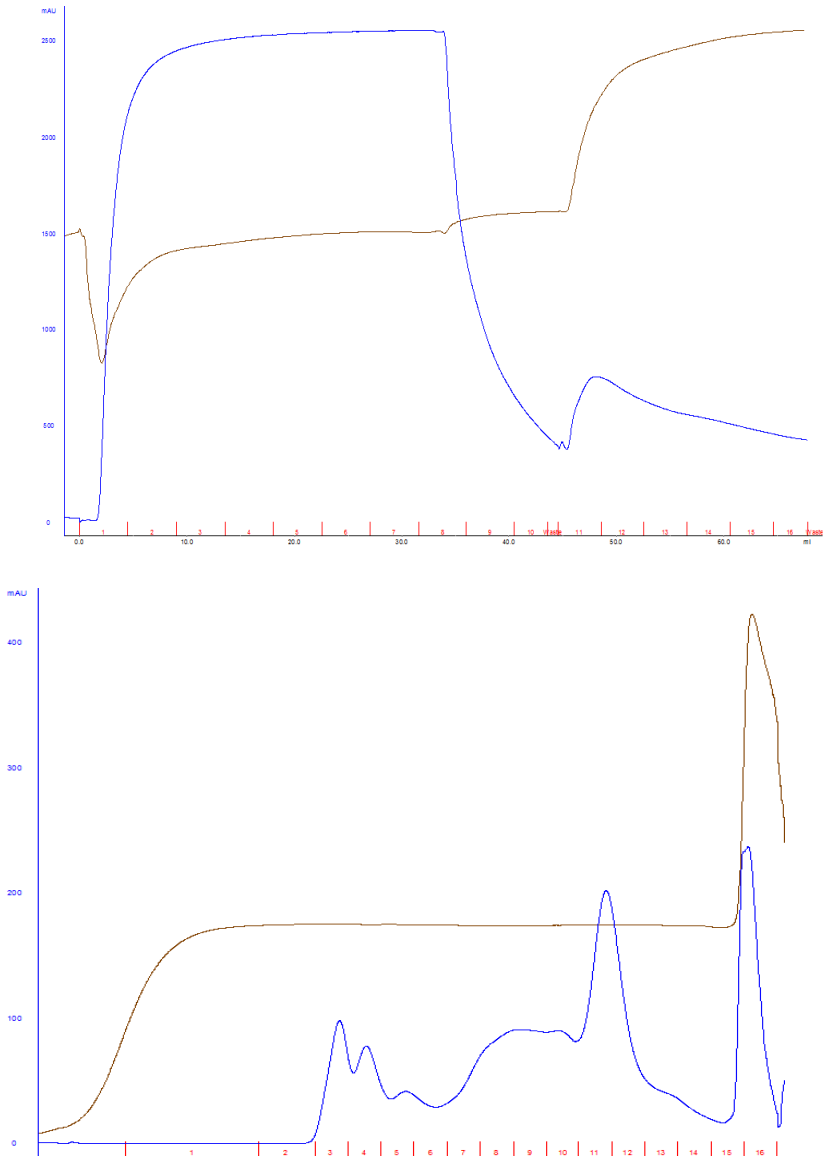

FIGURE 16. IMAC AND SEC ELUTION CHROMATOGRAM OF 3-OST 1 E90Q.

IMAC elution chromatogram (top). The bound protein was eluted with 100% IMAC B (fractions 11~16). The elution fractions were combined and concentrated for SEC chromatography.

SEC chromatogram on a superose 12 10/300 column (bottom). IMAC elution fractions were loaded on SEC column. The peak collected in fractions 11 and 12 contained a 33kDa band (based on SDS-PAGE shown in Figure 21). The blue traces indicate the UV absorption and orange traces indicate the conductivity readings that were recorded during the chromatography assays. The blue traces indicate the UV absorption and orange traces indicate the conductivity readings that were recorded during the chromatography assays.

APPENDIX E

SDS-PAGE GELS

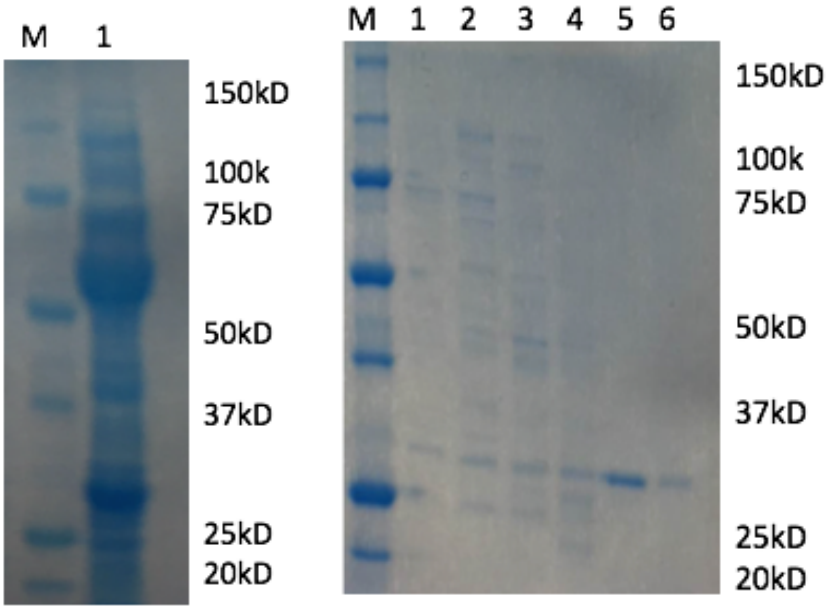

(A) (B)

FIGURE 17. SDS-PAGE GELS OF 3-OST 1 WT.

(A) The fractions obtained from the IMAC chromatography (Figure 10) that was prepared for the SEC chromatography. The obtained IMAC purification samples displayed a high level of non-specific proteins in the SDS-PAGE gels. Lane M = molecular weight ladder, lane 1= IMAC elution faction prepared for the SEC chromatography. (B) SEC purification (Figure 12) improved the purity of the purified proteins; the SDS PAGE gels showed that the non-specific proteins were separated from the 33kDa protein band that corresponds to the molecular weight of 3-OST 1 present in lane 5 and 6. Lane M = molecular weight ladder, lane 1= SEC elution faction #8, lane2= SEC elution faction #9, lane3= SEC elution faction #10, lane4= SEC elution faction #11, lane5= SEC elution faction #12, and lane 6= SEC elution faction #13.

FIGURE 18. SDS-PAGE GEL OF 3-OST 1 E90K.

SDS-GEL analysis of the fractions obtained from the SEC chromatography of E90K (Figure 13) where M = molecular weight ladder, lane2= IMAC elution faction prepared for the SEC chromatography, lane 3= SEC elution faction #11, and lane3= SEC elution faction #12. 33kDa protein band that corresponds to the molecular weight of 3-OST 1 were present in lane #2 and #3.

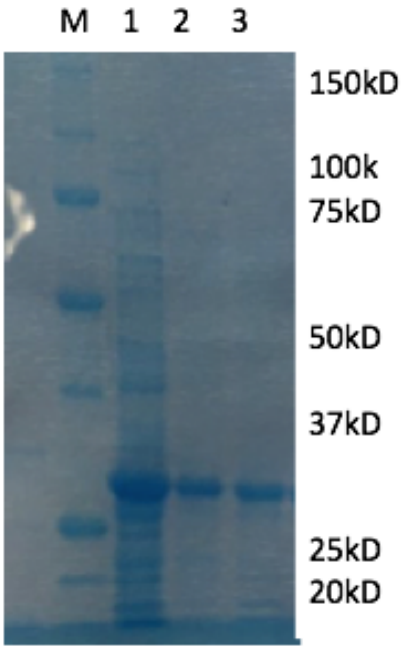

FIGURE 19. SDS-PAGE GEL OF 3-OST 1 E90H.

SDS-GEL analysis of the fractions obtained from the SEC chromatography of E90H (Figure 14) where lane1= elution faction #6, lane2= SEC elution faction #7, lane 3= SEC elution faction #8, lane 4= SEC elution faction #8, lane 5= SEC elution faction #9, lane 6= SEC elution faction #10, lane 7= SEC elution faction #11, lane 8= SEC elution faction #12, and lane M = molecular weight ladder. 33kDa protein band that corresponds to the molecular weight of 3-OST 1 were present in fractions 10 and 11.

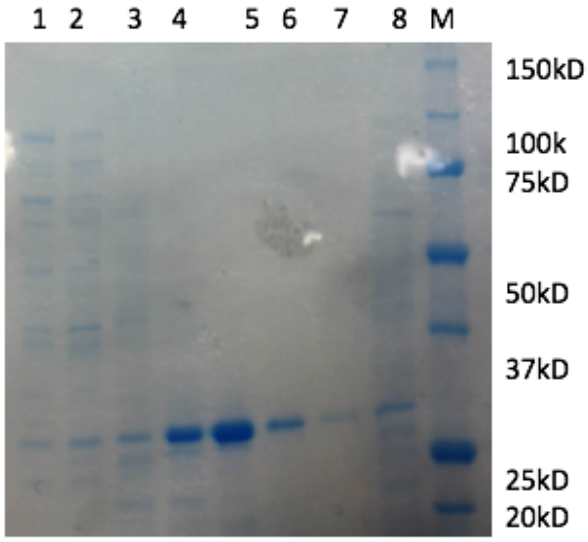

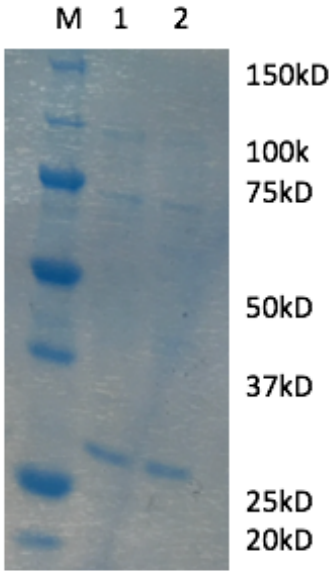

FIGURE 20. SDS-PAGE GEL OF 3-OST 1 E90R.

SDS-GEL analysis of the fractions obtained from the SEC chromatography of E90R (Figure 15) where lane M = molecular weight ladder, lane1= SEC elution faction #12, and lane2= SEC elution faction #13. 33kDa protein band that corresponds to the molecular weight of 3-OST were present in lane 1 and 2.

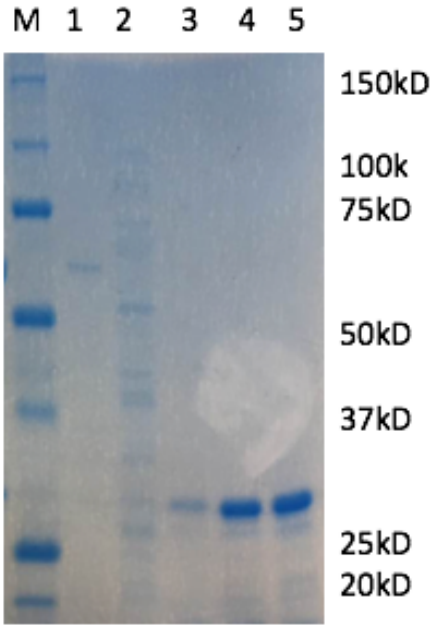

FIGURE 21. SDS-PAGE GEL OF 3-OST 1 E90Q.

SDS-GEL analysis of the fractions obtained from the SEC chromatography of E90Q (Figure 16) where M = molecular weight ladder, lane1= SEC elution faction #3, lane2= SEC elution faction #9, lane 3= SEC elution faction #10, lane 4= SEC elution faction #11, and lane 5= SEC elution faction #12. 33kDa protein band that corresponds to the molecular weight of 3-OST 1 was present in lane #4 and 5.

APPENDIX F

BLI SENSOGRAMS

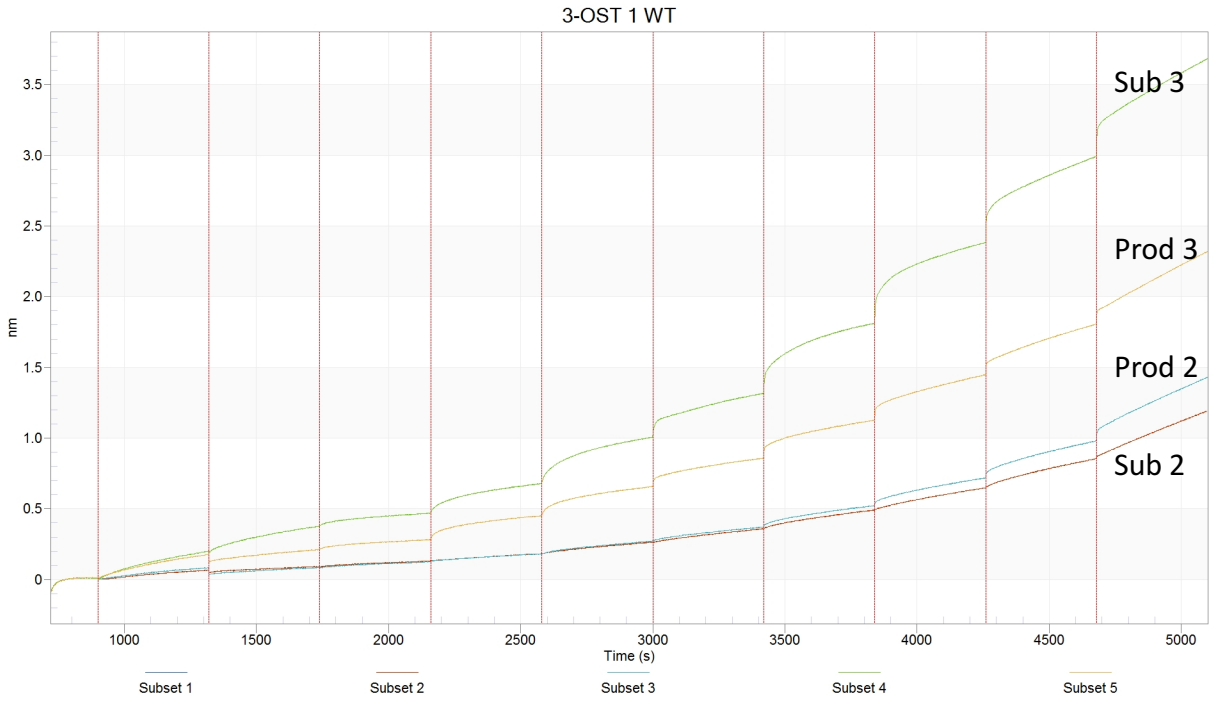

FIGURE 22. BLI SENSOGRAMS OF 3-OST 1 WT.

BLI measurements were obtained from Octet-RED96. Single cycle binding analysis was performed to monitor the association of the 3-OST1 WT with the immobilized HS fragments. Biotinylated HS fragments were immobilized on the biosensor and multiple concentrations of the 3-OST 1analyte were prepared in phosphate-buffered saline. The sensor signals were referenced using a parallel buffer blank subtraction and the baseline was aligned to the y-axis by the by the Savitzky-Goaly filtering function of the data analysis software

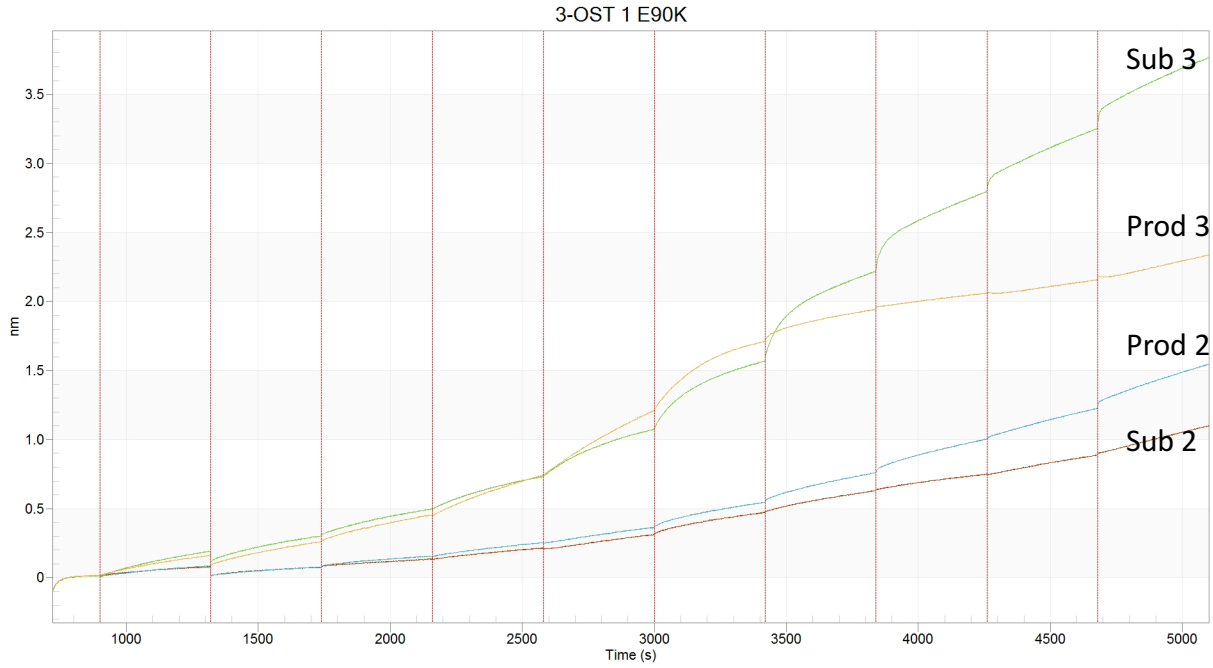

FIGURE 23. BLI SENSOGRAMS OF 3-OST 1 E90K.

BLI measurements were obtained from Octet-RED96. Single cycle binding analysis was performed to monitor the association of the 3-OST1 E90K with the immobilized HS fragments. Biotinylated HS fragments were immobilized on the biosensor and multiple concentrations of the 3-OST 1analyte were prepared in phosphate-buffered saline. The sensor signals were referenced using a parallel buffer blank subtraction and the baseline was aligned to the y-axis by the by the Savitzky-Goaly filtering function of the data analysis software

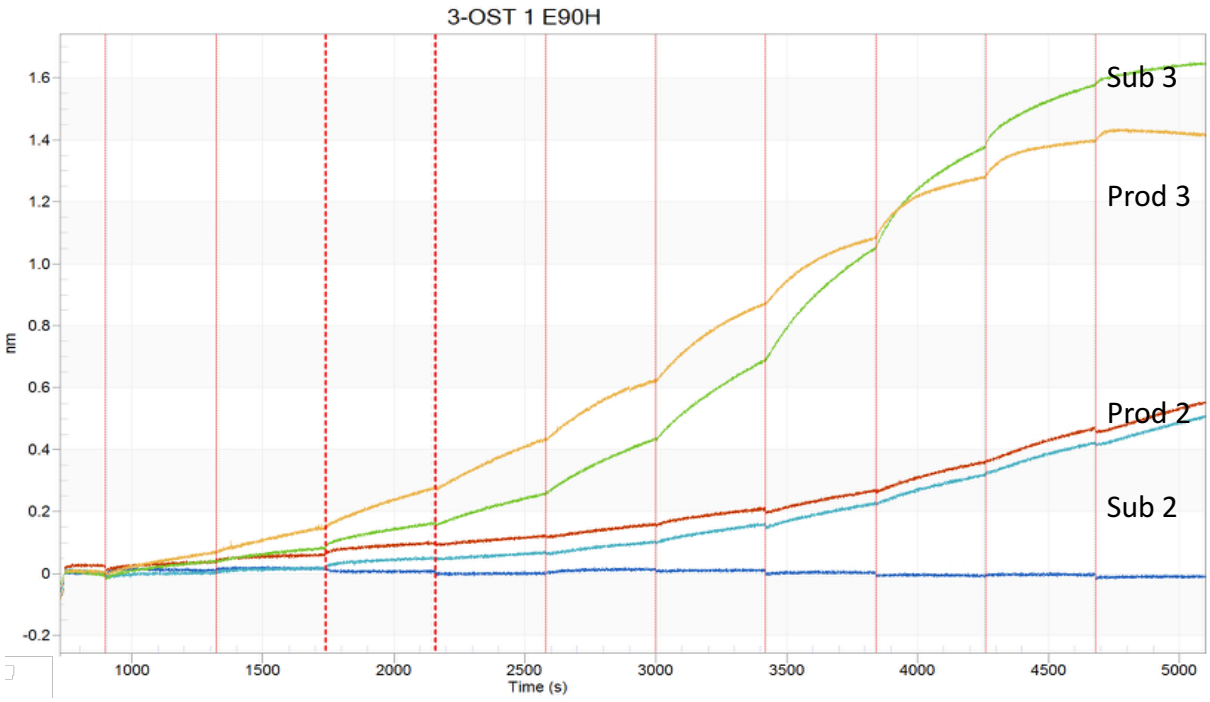

FIGURE 24. BLI SENSOGRAMS OF 3-OST 1 E90H.

BLI measurements were obtained from Octet-RED96. Single cycle binding analysis was performed to monitor the association of the 3-OST1 E90H with the immobilized HS fragments. Biotinylated HS fragments were immobilized on the biosensor and multiple concentrations of the 3-OST 1analyte were prepared in phosphate-buffered saline. The sensor signals were referenced using a parallel buffer blank subtraction and the baseline was aligned to the y-axis by the by the Savitzky-Goaly filtering function of the data analysis software

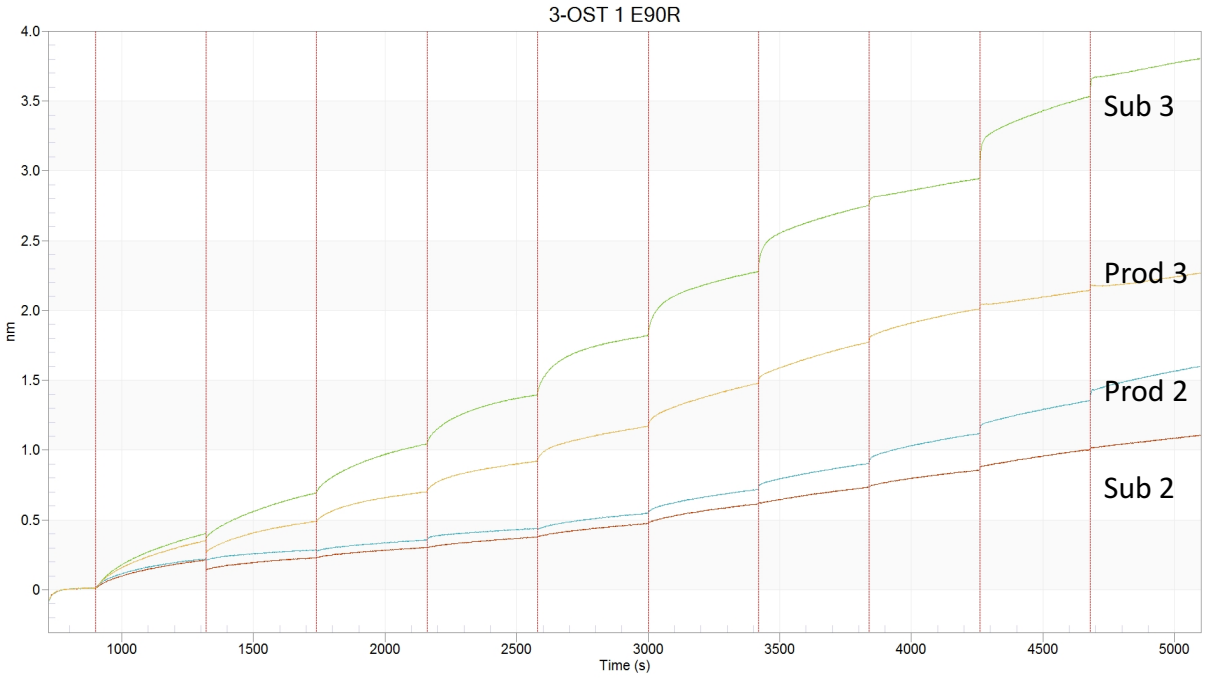

FIGURE 25. BLI SENSOGRAMS OF 3-OST 1 E90R.

BLI measurements were obtained from Octet-RED96. Single cycle binding analysis was performed to monitor the association of the 3-OST1 E90R with the immobilized HS fragments. Biotinylated HS fragments were immobilized on the biosensor and multiple concentrations of the 3-OST 1analyte were prepared in phosphate-buffered saline. The sensor signals were referenced using a parallel buffer blank subtraction and the baseline was aligned to the y-axis by the by the Savitzky-Goaly filtering function of the data analysis software

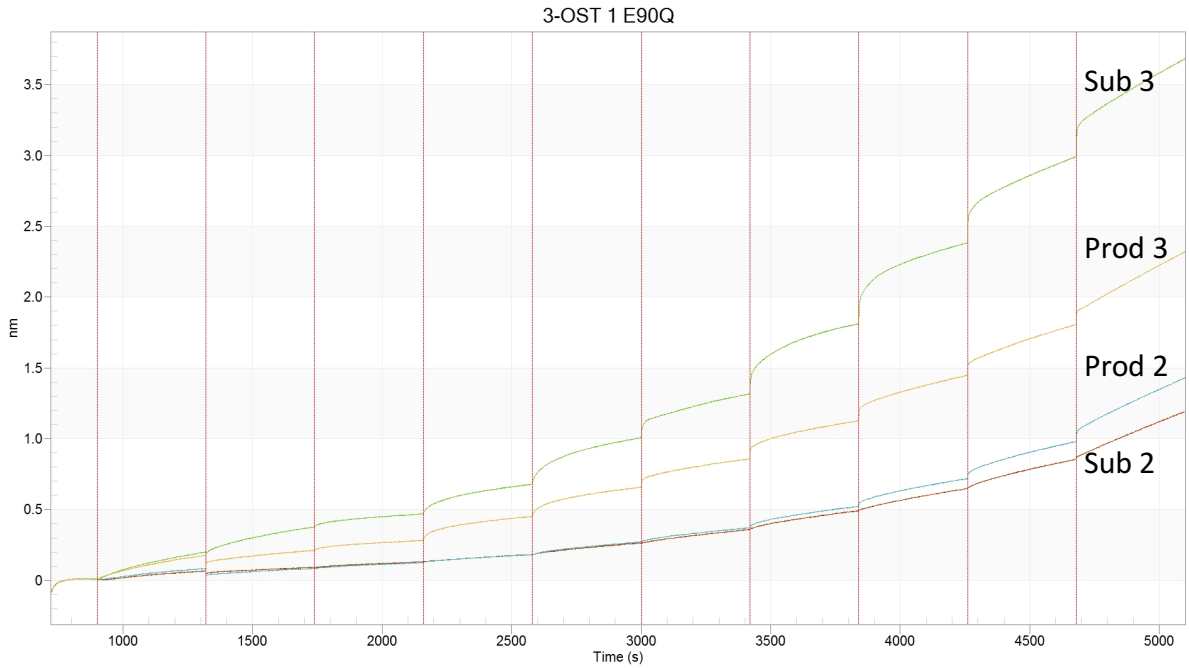

FIGURE 26. BLI SENSOGRAMS OF 3-OST 1 E90Q.

BLI measurements were obtained from Octet-RED96. Single cycle binding analysis was performed to monitor the association of the 3-OST1 E90Q with the immobilized HS fragments. Biotinylated HS fragments were immobilized on the biosensor and multiple concentrations of the 3-OST 1analyte were prepared in phosphate-buffered saline. The sensor signals were referenced using a parallel buffer blank subtraction and the baseline was aligned to the y-axis by the by the Savitzky-Goaly filtering function of the data analysis software

APPENDIX G

BLI RAW DATA AND K_D VALUES

Biotinylated HS fragments on biosensor binding to 3-OST 1 WT (in two-fold dilution series)				
WT (uM)	Sub 2	Prod 2	Sub 3	Prod 3
0.008	0.064	0.082	0.198	0.175
0.015	0.091	0.084	0.376	0.211
0.031	0.130	0.126	0.468	0.281
0.063	0.181	0.180	0.677	0.450
0.125	0.263	0.270	1.005	0.656
0.250	0.358	0.370	1.315	0.857
0.500	0.490	0.521	1.809	1.124
1.000	0.646	0.717	2.380	1.446
2.000	0.852	0.977	2.987	1.803
4.000	1.187	1.425	3.677	2.313
BEST-FIT VALUES OBTAINED FROM PRISM 7.03				
	Sub 2	Prod 2	Sub 3	Prod 3
Bmax	1.194	1.729	3.661	2.151
Kd	1.112	1.792	0.4939	0.4675

TABLE 6. BLI RAW DATA AND K_D VALUES FOR 3-OST 1 WT.

BLI measurements were obtained from Octet-RED96. Single cycle binding analysis was performed to monitor the association of the 3-OST1. The obtained raw data was processed by fitting the steady-state binding data to a 1:1 Langmuir binding model using Prism software (version 7.03, GraphPad Software, La Jolla, USA).

Biotinylated HS fragments on biosensor binding to 3-OST 1 E90K (in two-fold dilution series)				
E90K (uM)	Sub 2	Prod 2	Sub 3	Prod 3
0.008	0.077	0.084	0.189	0.160
0.015	0.074	0.073	0.300	0.259
0.031	0.134	0.156	0.495	0.453
0.063	0.213	0.252	0.729	0.740
0.125	0.309	0.362	1.071	1.204
0.250	0.473	0.545	1.566	1.708
0.500	0.628	0.759	2.214	1.940
1.000	0.748	1.001	2.791	2.059
2.000	0.887	1.224	3.248	2.156
4.000	1.096	1.542	3.760	2.333
BEST-FIT VALUES OBTAINED FROM PRISM 7.03				
	Sub 2	Prod 2	Sub 3	Prod 3
Bmax	0.896	1.461	3.728	2.177
Kd	0.349	0.595	0.359	0.112

TABLE 7. BLI RAW DATA AND K_D VALUES FOR 3-OST 1 E90K.

BLI measurements were obtained from Octet-RED96. Single cycle binding analysis was performed to monitor the association of the 3-OST1 E90K. The obtained raw data was processed by fitting the steady-state binding data to a 1:1 Langmuir binding model using Prism software (version 7.03, GraphPad Software, La Jolla, USA).

`

Biotinylated HS fragments on biosensor binding to 3-OST 1 E90H (in two-fold dilution series)				
E90H (uM)	Sub 2	Prod 2	Sub 3	Prod 3
0.008	0.005	-0.013	0.030	0.053
0.015	0.024	-0.016	0.020	0.134
0.031	0.070	0.026	0.109	0.274
0.063	0.099	0.050	0.209	0.435
0.125	0.124	0.072	0.373	0.613
0.250	0.177	0.132	0.629	0.863
0.500	0.243	0.206	0.998	1.082
1.000	0.345	0.308	1.335	1.290
2.000	0.450	0.408	1.533	1.404
4.000	0.540	0.500	1.611	1.431
BEST-FIT VALUES OBTAINED FROM PRISM 7.03				
	Sub 2	Prod 2	Sub 3	Prod 3
Bmax	0.4443	0.539	1.661	1.305
Kd	1.116	2.601	0.4725	0.159

TABLE 8. BLI RAW DATA AND K_D VALUES FOR 3-OST 1 E90H.

BLI measurements were obtained from Octet-RED96. Single cycle binding analysis was performed to monitor the association of the 3-OST1 E90H. The obtained raw data was processed by fitting the steady-state binding data to a 1:1 Langmuir binding model using Prism software (version 7.03, GraphPad Software, La Jolla, USA).

Biotinylated HS fragments on biosensor binding to 3-OST 1 E90R (in two-fold dilution series)				
E90R (uM)	Sub 2	Prod 2	Sub 3	Prod 3
0.008	0.212	0.220	0.399	0.348
0.015	0.229	0.285	0.691	0.490
0.031	0.302	0.357	1.042	0.700
0.063	0.377	0.438	1.393	0.920
0.125	0.474	0.547	1.819	1.170
0.250	0.613	0.717	2.276	1.475
0.500	0.734	0.903	2.751	1.772
1.000	0.855	1.117	2.943	2.009
2.000	1.002	1.352	3.530	2.143
4.000	1.104	1.598	3.802	2.265
BEST-FIT VALUES OBTAINED FROM PRISM 7.03				
	Sub 2	Prod 2	Sub 3	Prod 3
Bmax	0.826	1.304	3.378	2.001
Kd	0.094	0.209	0.103	0.079

TABLE 9. BLI RAW DATA AND K_D VALUES FOR 3-OST 1 E90R.

BLI measurements were obtained from Octet-RED96. Single cycle binding analysis was performed to monitor the association of the 3-OST1 E90R. The obtained raw data was processed by fitting the steady-state binding data to a 1:1 Langmuir binding model using Prism software (version 7.03, GraphPad Software, La Jolla, USA).

`

Biotinylated HS fragments on biosensor binding to 3-OST 1 E90Q (in two-fold dilution series)				
E90Q (uM)	Sub 2	Prod 2	Sub 3	Prod 3
0.008	0.0905	0.0844	0.3758	0.2109
0.015	0.1303	0.1255	0.4682	0.2813
0.031	0.181	0.1801	0.6771	0.4497
0.063	0.263	0.2704	1.0049	0.6564
0.125	0.3576	0.3702	1.3152	0.8566
0.250	0.4902	0.5205	1.8092	1.1244
0.500	0.646	0.7165	2.3799	1.4456
1.000	0.8523	0.9771	2.9871	1.8027
2.000	0.0905	0.0844	0.3758	0.2109
4.000	0.1303	0.1255	0.4682	0.2813
BEST-FIT VALUES OBTAINED FROM PRISM 7.03				
	Sub 2	Prod 2	Sub 3	Prod 3
Bmax	0.4443	0.539	1.661	1.305
Kd	1.116	2.601	0.4725	0.159

TABLE 10. BLI RAW DATA AND K_D VALUES FOR 3-OST 1 E90Q.

BLI measurements were obtained from Octet-RED96. Single cycle binding analysis was performed to monitor the association of the 3-OST1 E90Q. The obtained raw data was processed by fitting the steady-state binding data to a 1:1 Langmuir binding model using Prism software (version 7.03, GraphPad Software, La Jolla, USA).

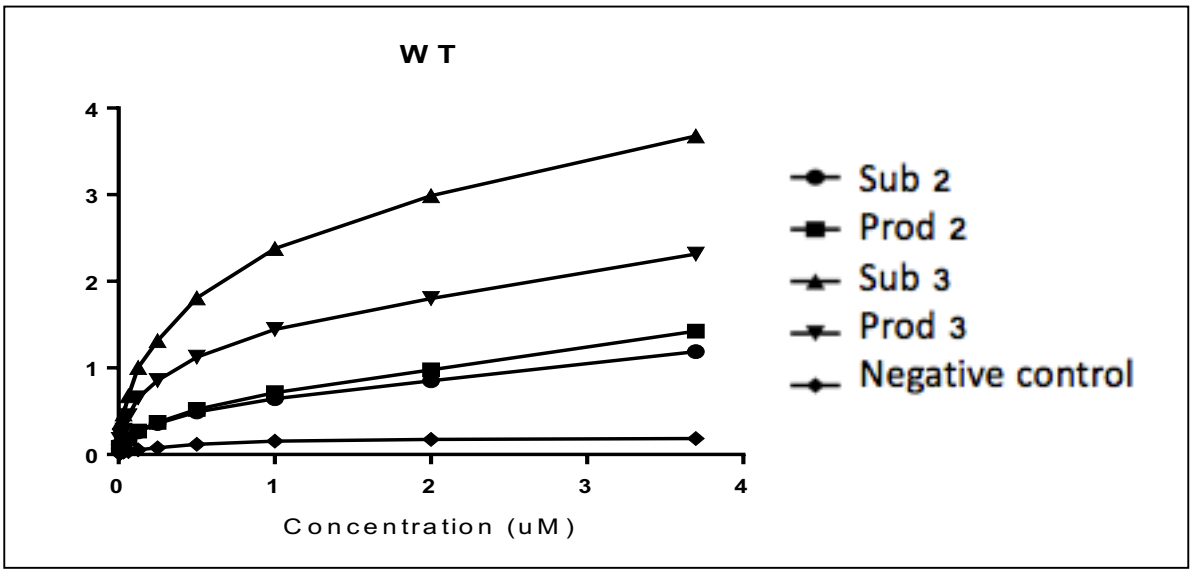

FIGURE 27. EQUILIBRIUM BINDING ANALYSIS OF 3-OST 1 WT.

BLI measurements were obtained from Octet-RED96. Single cycle binding analysis was performed to monitor the association of the 3-OST1. The obtained raw data was processed by Prism software (version 7.03, GraphPad Software, La Jolla, USA). In order to account for the non-specific interactions, the binding of the protein to the bare biosensor (no glycan immobilized on the biosensor) was also measured and subtracted from the sensor's signals.

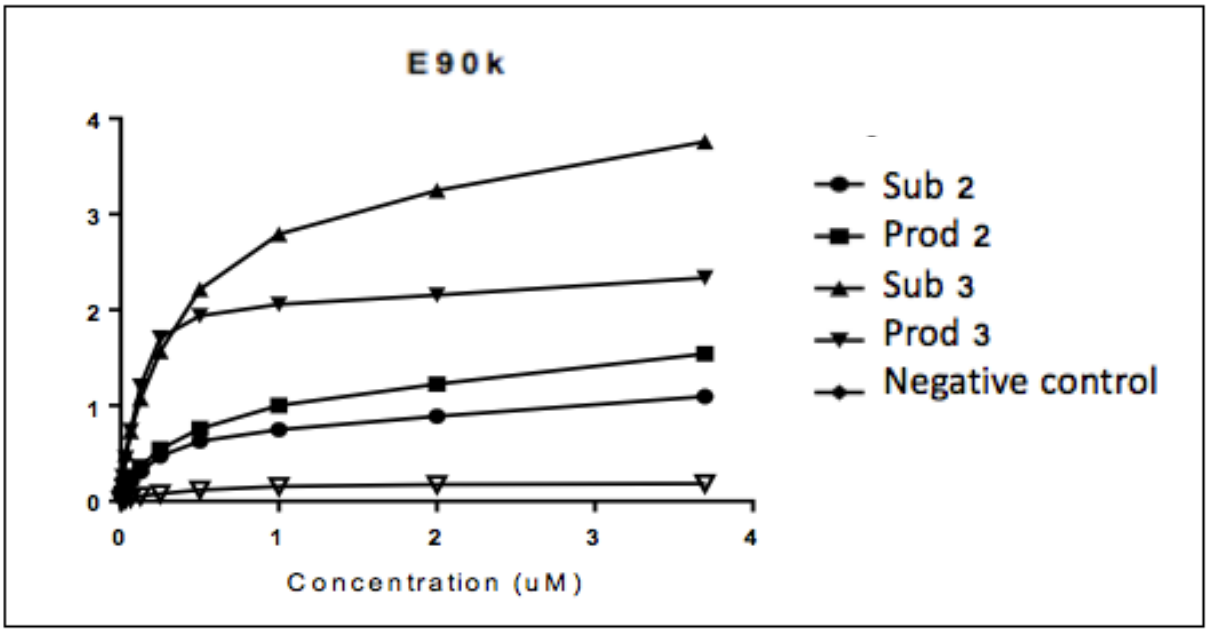

FIGURE 28. EQUILIBRIUM BINDING ANALYSIS OF 3-OST 1 E90K.

BLI measurements were obtained from Octet-RED96. Single cycle binding analysis was performed to monitor the association of the 3-OST1 E90K. The obtained raw data was processed by Prism software (version 7.03, GraphPad Software, La Jolla, USA). In order to account for the non-specific interactions, the binding of the protein to the bare biosensor (no glycan immobilized on the biosensor) was also measured and subtracted from the sensor's signals.

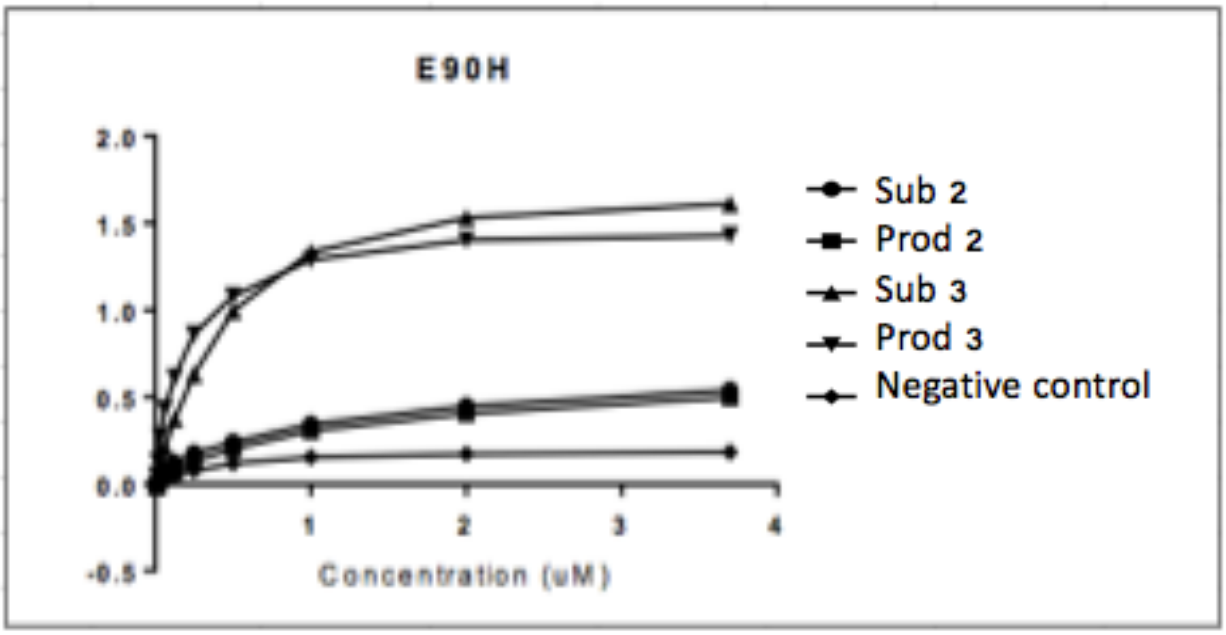

FIGURE 29. EQUILIBRIUM BINDING ANALYSIS OF 3-OST 1 E90H.

BLI measurements were obtained from Octet-RED96. Single cycle binding analysis was performed to monitor the association of the 3-OST1 E90H. The obtained raw data was processed by Prism software (version 7.03, GraphPad Software, La Jolla, USA). In order to account for the non-specific interactions, the binding of the protein to the bare biosensor (no glycan immobilized on the biosensor) was also measured and subtracted from the sensor's signals

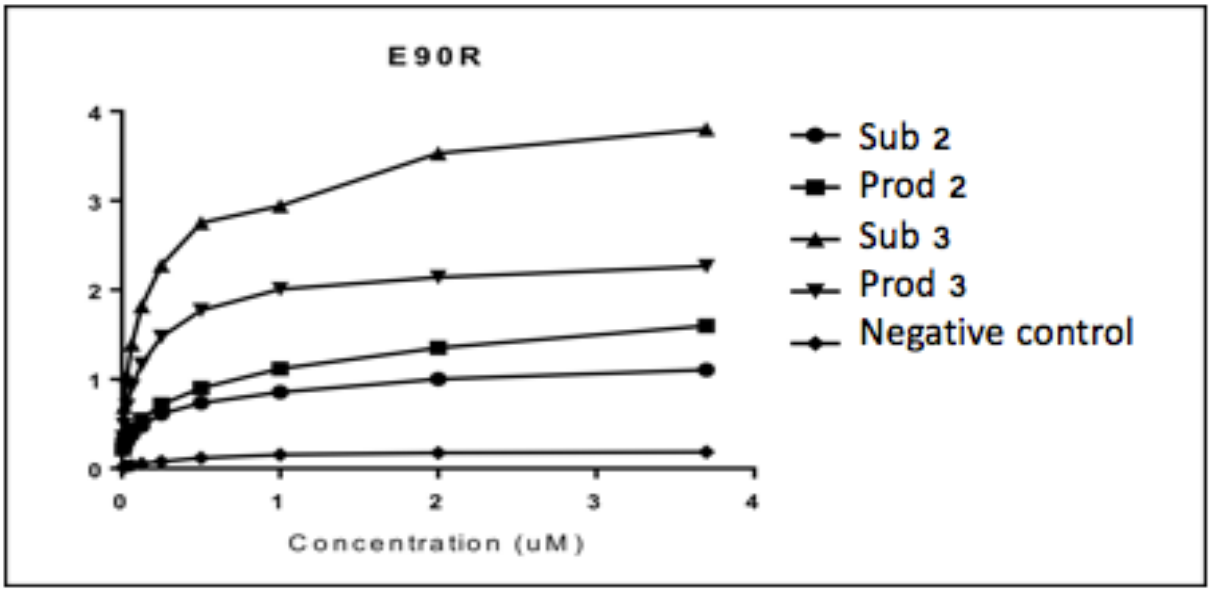

FIGURE 30. EQUILIBRIUM BINDING ANALYSIS OF 3-OST 1 E90R.

BLI measurements were obtained from Octet-RED96. Single cycle binding analysis was performed to monitor the association of the 3-OST1 E90R. The obtained raw data was processed by Prism software (version 7.03, GraphPad Software, La Jolla, USA). In order to account for the non-specific interactions, the binding of the protein to the bare biosensor (no glycan immobilized on the biosensor) was also measured and subtracted from the sensor's signals

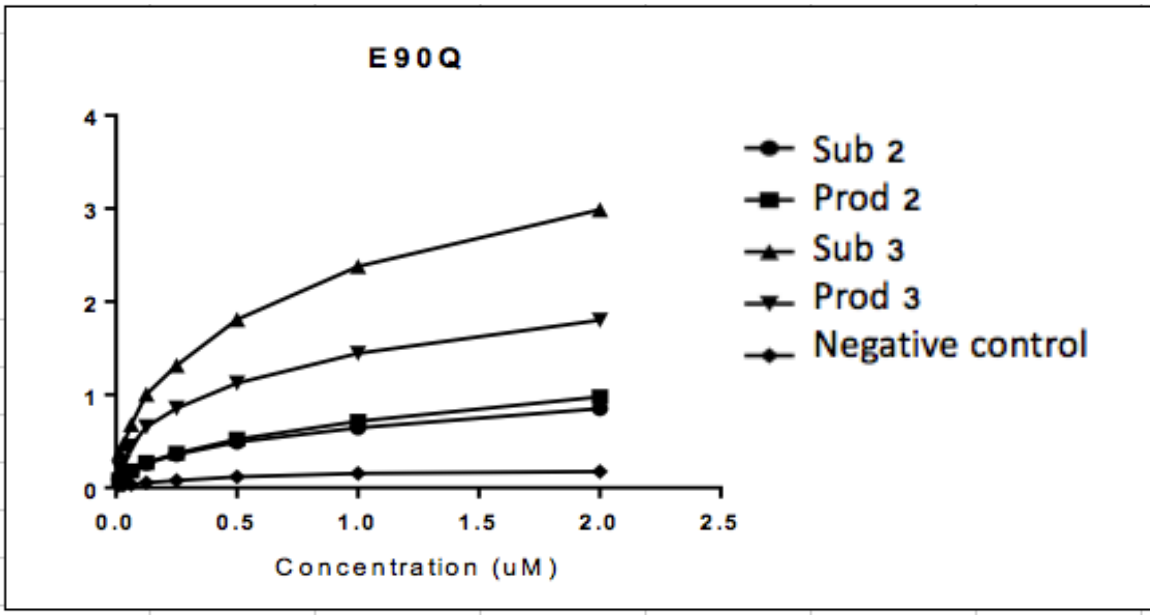

FIGURE 31. EQUILIBRIUM BINDING ANALYSIS OF 3-OST 1 E90Q.

BLI measurements were obtained from Octet-RED96. Single cycle binding analysis was performed to monitor the association of the 3-OST1 E90Q. The obtained raw data was processed by Prism software (version 7.03, GraphPad Software, La Jolla, USA). In order to account for the non-specific interactions, the binding of the protein to the bare biosensor (no glycan immobilized on the biosensor) was also measured and subtracted from the sensor's signals